Ecological Indicators 150 (2023) 110247

Contents lists available at ScienceDirect

Ecological Indicators

journal homepage: www.elsevier.com/locate/ecolind

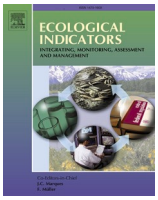

Divergent vegetation variation and the response to extreme climate events in the National Nature Reserves in Southwest China, 1961–2019

Ping Wang [a], Qingping Cheng [b,c,*], Hanyu Jin [b]

[a] Faculty of Geography, Yunnan Normal University, Kunming 650500, China
[b] School of Geography and Ecotourism, Southwest Forestry University, Kunming 650224, China
[c] Southwest Research Centre for Eco-civilization, National Forestry and Grassland Administration, Kunming 650224, China

ARTICLE INFO

Keywords:
National Nature Reserves
Extreme climate events
Impact and response
Southwest China

ABSTRACT

Southwest China (SWC) is a critical hotspot of biodiversity and highly sensitive to climate change. To better protect biodiversity, many National Nature Reserves have been established to maintain viable populations of species and minimize their habitat loss. However, the response of the normalized difference vegetation index (NDVI) in National Nature Reserves to extreme climate events has not been described. We analyzed NDVI changes and made several key observations: (1) from 1998 to 2019, annual average NDVI trends of 0.00421 yr^{-1}, 0.00514 yr^{-1}, and 0.00529 yr^{-1} were significantly increasing and NDVI values more than 0.8 were mainly concentrated at 1049–2349 m, 947–2547 m, 617–2817 m, in the National Nature Reserves of Hengduan Mountain (NNRHDM), Sichuan basin (NNRSCB), and Yunnan-Guizhou Plateau (NNRYGP), respectively. The change trends in different altitude bins were more significant in the NNRYGP; (2) extreme cold (warm) indices significantly decreased (increased) in the NNRHDM, NNRSCB and NNRYGP, extreme precipitation indices increased in the NNRHDM, and decreased in the NNRSCB and NNRYGP; (3) the combination of extreme temperature indices can better explain NDVI change in the NNRSCB and NNRYGP, and the combination of extreme temperature and precipitation indices can better explain the NDVI change in the NNRHDM on the monthly scale. Overall, the NDVI green trend is more obvious in the NNRYGP than in the NNRHDM and NNRSCB, and is more sensitive to extreme climate change, especially extreme temperature. Our findings showed that although the National Nature Reserves have achieved remarkable results in conservation, future work should focus on the development of adaptation and alleviation strategies to prevent extreme climate events (especially extreme temperature events) that could promote vegetation degradation in these sensitive areas.

1. Introduction

Climate conditions determine differences between biological communities and habitat types (Woodward et al., 2004), limiting the distribution range of species (Chen et al., 2011) and controlling patterns of biodiversity (Kreft and Jetz, 2007). Thus, climate change may cause species to migrate, expand, contract (Scheffers et al., 2016), and even restructure large areas of biological communities (Williams and Jackson, 2007). Therefore, there is significant interest in understanding the speed and stability of changes to the survival space of species in the context of climate change and whether current climate types will disappear and new climate types will emerge (Loarie et al., 2009; Ohlemüller, 2011; Watson et al., 2013; Garcia et al., 2014; Gao et al., 2019; Elsen et al., 2020; Asamoah et al., 2021; Shrestha et al., 2021; Wu et al., 2023). Vegetation dynamics are key drivers of terrestrial ecosystems (Watson et al., 2013) with crucial roles in energy exchange, nutrient cycles, hydrological cycles, carbon sequestration, soil erosion, and water quality (Ɓegúe et al., 2011; Smith et al., 2014; Ouyang et al., 2018; Xu et al., 2020). Therefore, analyzing climate change, especially extreme climate change, vegetation dynamics, and the impact of climate change on vegetation dynamics, is crucial to understand the overall effects of climate change on ecosystems (Gao et al., 2021).

Many climatic extremes are increasing in frequency and intensity, including floods, droughts, rainstorms, and heatwaves (Fischer et al., 2013; Meehl et al., 2009; Perkins et al., 2012; Rahmstorf and Coumou, 2011). These changes have significant effects on agriculture, industry, economics, and ecology (Jones et al., 2015; Peng et al., 2013; Siepielski et al., 2017; Zhang et al., 2019). Extreme climate events are predicted to

* Corresponding author at: School of Geography and Ecotourism, Southwest Forestry University, Kunming 650224, China.
E-mail address: qpchengtyli@foxmail.com (Q. Cheng).

https://doi.org/10.1016/j.ecolind.2023.110247
Received 4 July 2022; Received in revised form 24 March 2023; Accepted 10 April 2023
Available online 19 April 2023

become even more frequent in the near future (Lavell et al., 2012; Donat et al., 2016; Pfahl et al., 2017). Therefore, it is essential to understand changes in frequency, duration, intensity, and spatial and temporal variability of extreme climate events at different regions and different scales, as well as their environmental impacts (Cheng et al., 2021). Efforts have been made to understand these changes at the global scale (Alexander et al., 2006; Westra et al., 2013; Papalexiou et al., 2018; Papalexiou and Montanari 2019) and in Central Asia (Chen et al., 2018), Europe (Fioravanti et al., 2016), the Indo-Pacific region (Caesar et al., 2011), West Africa (Panthou et al., 2012), the United States (Schoof and Robeson, 2016; Xue et al., 2017) and China (Sun et al., 2014; Chen and Sun,2017; Zhou and Liu, 2018).

The normalized difference vegetation index (NDVI) is widely used to represent vegetation greenness, as it provides a reliable measure of photosynthesis (vegetation activity) based on the infrared and near-infrared bands of remote sensing imagery (Piao et al., 2006). NDVI is closely linked to the functional traits of vegetation and is strongly correlated with leaf area, photosynthetically active radiation absorption, and vegetation productivity (Wei et al., 2018). As a result, NDVI has been widely employed to measure spatiotemporal trends in vegetation, including phenological and altitudinal differences at the global and sub-region scale to assess the impacts of climate change and human activities (Peng et al., 2013; Wu et al., 2015; Lamchin et al., 2018; Gao et al., 2019; Shen et al., 2021; Sun et al., 2021). Protected areas play crucial roles in maintaining species survival and minimizing the habitat loss of species populations, so there is strong interest in analyzing the vegetation dynamics of protected areas (Li et al., 2016; Gao et al., 2021; Li et al., 2021; Ma et al., 2022), particularly to assess conservation effectiveness (Li et al., 2021; Shrestha et al., 2021; Li and Song, 2022), the impact of different management strategies on conservation outcomes (Brandt et al., 2015), the sufficiency of protected area coverage (Wu et al., 2023), and the functions of protected areas as thermal buffers (Xu et al., 2022) and for social benefits of humans (Naidoo et al., 2019). Protected areas may have climate vulnerability, and protection is expected to decline in cold and warm climates and increase in cool and hot climates over a wide range of precipitation by 2070 (Elsen et al., 2020). More than one-quarter of the world's protected areas (~27 %) are located in regions that are predicted to experience both high rates of climate change and land-use change by 2050 (Asamoah et al., 2021). In China, nearly 10 % of protected areas are highly threatened and about one-fifth of protected areas are hotspots of climate and anthropogenic vulnerabilities (Shrestha et al., 2021). Therefore, it is urgent to investigate the vegetation dynamics and the response to extreme climates in protected areas, especially in the southwestern region of China, which is considered a hotspot of global biodiversity.

In recent years, extreme climate events have occurred frequently in Southwest China (SWC), with serious damage to the economy, ecosystem, and environment. Therefore, there is significant research interest in the temporal and spatial variation characteristics and impact mechanism of extreme climate events (Cheng et al., 2019; Ding et al., 2020; Liu et al., 2014; Qin et al., 2015), and vegetation dynamic change characteristics and influencing factors for climate change and human activities in SWC (Gu et al., 2018; Huo and Sun, 2021; Jiang et al., 2021a, b; Li et al., 2019; Liu et al., 2018, 2020; Ouyang et al., 2020; Shao et al., 2021; Song et al., 2019; Yan et al., 2021; Yin et al., 2020). However, few studies have focused on extreme climate change in National Nature Reserves and its impact on vegetation in China and sub-regions. Shrestha et al (2021) used a multidimensional approach incorporating species, climate, and anthropogenic vulnerabilities to assess the threat levels in over 2500 protected areas in China. Li et al (2016) found vegetation greening rate decreased significantly as elevation increased, with a threshold elevation of approximately 3000 m. Li et al (2021) observed that the average elevation for negative relationships of vegetation elevation was higher than that for positive relationships between elevation and NDVI in the Wuyi Mountains National Nature Reserve in Fujian province, China. Gao et al (2021) found vegetation–climate relationships demonstrate a degree of spatial heterogeneity driven by variability in climate factors and ecosystems in the Qilian Mountain Nature Reserve in Northwest China. However, little attention has been paid to extreme climate change and its impact on NDVI in National Nature Reserves in SWC (NNRSWC), important areas of global biodiversity and carbon sequestration. To address this gap, the extreme climate change characteristics and its impact on NDVI were investigated. The main objectives of this study were as follows: (1) to assess spatiotemporal changes of extreme climate indices between 1961 and 2019; (2) to identify the spatiotemporal and altitudinal changes in NDVI from 1998 to 2019; and (3) to investigate the relationships between annual/month NDVI with extreme climate indices from 1998 to 2019. The results of this research should provide scientific reference about vegetation adaptation to extreme climate change and can guide policies to facilitate effective biodiversity conservation in NNRSWC.

2. Data and methods

2.1. Study area

SWC is the area east of the Tibetan Plateau and mainly includes Sichuan, Yunnan, and Guizhou provinces, and Chongqing municipality. SWC encompasses a large geographic area with complex landscapes, including plateau (Yunnan–Guizhou Plateau, YGP), mountain (Hengduan Mountains, HDM), hills (eastern Sichuan hills), and basin (Sichuan Basin, SCB; the eastern Sichuan hills are included within the SCB region in this study (Sun et al., 2016)). There are four main source regions for precipitation moisture in the SWC: the southwest monsoon, westerlies, local, and southeast monsoon regions. The southwest monsoon region is the largest moisture source, contributing more than half of the precipitation moisture (Zhang and Wu, 2021). A typical subtropical monsoon climate prevails across SWC, with a clearly defined dry/wet season with a rainy season that usually begins in April and ends in October (Sun et al., 2016). SWC is vulnerable to floods during the rainy season and droughts during the dry season, which can have great societal and economic effects (Sun et al., 2016) and different effects on vegetation (Song et al., 2019).

2.2. Data resource

Daily temperature and precipitation data from January 1961 to February 2020 were obtained from the China Meteorological data sharing service network (http://data.cma.cn/) version V3.0. The homogeneity and reliability of the daily meteorological data was rigorously assessed by the National Meteorological Information Center, China Meteorological Administration before data release. These data account for station relocation, instrument replacement, and changes of the surrounding environment of the stations, to more realistically reflect natural climate change. Stations missing more than 5 % of daily data during the time period (1961–2019) were removed. For stations missing<5 % of daily measurement, missing values were replaced via linear interpolation from the average daily observations for the surrounding 4 days (Cheng et al., 2023). The digital elevation model (DEM) data were taken with 1000 m resolution and were obtained from the Data Centre for Resources and Environmental Sciences (http://www.resdc.cn/data). The annual and monthly NDVI spatial distribution data set is satellite remote sensing data of SPOT/VEGETATION based on continuous time series (1998–2019), 1:1000000 vegetation map, and vector data of 64 NNRSWC. We further distinguish three areas of NNRHDM, NNRSCB, and NNRYGP, described in detail in Table S1). These data were obtained from the resource and environmental science data center of the Chinese Academy of Sciences (https://www.resdc.cn).

2.3. Methods

2.3.1. Extreme climate indices

A total of 18 extreme temperature indices and 11 extreme precipitation indices (Table S2) from Expert Team Climate Change Detection and Indices (ETCCDI) (https://etccdi.pacificclimate.org/index.shtml) were calculated using the R package "*RClimDex*" and were used to analyze the spatial distribution and temporal trends of extreme climate events.

2.3.2. Selection criteria of meteorological stations and different buffer NDVI extraction

There are no meteorological stations within the NNRSWC, so nearest neighbor analysis in the ArcGIS 10.8 analysis tool was used to extract the nearest meteorological station of each reserve from more than 400 stations in the SWC (data from a total of 98 stations were extracted (Table S3)). NDVI values for different buffer zones (2 km, 5 km, or 10 km) were extracted for each station for analysis. We choose 2, 5, and 10 km as buffer distances instead of selecting a continuous range of 1–10 km primarily because the average NDVI values extracted at intervals of every 1 km are unlikely to differ significantly. If we were to extract the average NDVI values at every 1 km interval, it could lead to redundant analysis. Furthermore, we did not choose buffer distances exceeding 10 km primarily because most protected areas are not very large. Therefore, considering these factors, we mainly selected buffer distances of 2, 5, and 10 km.

2.3.3. Additional analysis methods

Sen's slope estimator and the Modified Mann–Kendall test using trend-free Pre-Whitening method and Pettitt method were used to determine the trends, slope, and abrupt shifts (Mann 1945; Theil 1950; Sen 1968; Pettitt, 1979; Yue and Wang, 2002).

Stepwise multiple linear regression models analyse the relation between a dependent variable (i.e., NDVI) and explanatory variables (extreme climate indices) by fitting a linear equation using observed data. These models use criteria to automatically select explanatory variables, such as Akaike information criterion (AIC) and Bayesian information criterion (BIC). The adj-R^2 is usually interpreted as the percentage of the total variation of the dependent variable (e. g., NDVI) that can be explained by all independent variables (e.g., extreme climate indices) adjusted for the number of variables used (Wen et al., 2017; Xu et al., 2003). Here, adj-R^2 was estimated by an *F*-test at a significance level of 0.05. Multicollinearity refers to a situation in which two or more explanatory variables in a multiple regression model are highly linearly related and can be detected using the variance inflation factor (VIF). VIFs were confirmed to be below 10 (Kutner et al., 2004), and insignificant variables (i.e., *p*-values $\geq$ 0.05) were removed in a stepwise procedure. All processes were implemented in Matlab20a. More detailed information is presented in Liu et al. (2018) and Liu et al. (2021).

In addition, Spearman correlation analysis was performed between annual/month NDVI values with extreme climate indices in different buffer areas. The Pearson correlation coefficient has been previously used to reveal the correlation between extreme climate indices and NDVI (Gao et al., 2021; Ying et al., 2020; Shen et al., 2021). Pearson correlation coefficient requires both variables to be continuous numerical variables, while Spearman correlation coefficient can be used for any data type, including continuous numerical variables and ordinal variables (such as ranking or categorical variables). The Spearman correlation coefficient is a nonparametric correlation coefficient used to measure the strength of a monotonic relationship between two variables. It does not require a linear relationship between variables, but the Spearman correlation coefficient can be used if the relationship between variables must be monotonic (i.e., when the value of one variable increases, the value of another variable also increases or decreases). Spearman correlation coefficients range between −1 and + 1, where −1 represents a perfect negative correlation, +1 represents a perfect positive correlation, and 0 represents no monotonic relationship.

3. Results

3.1. Spatial-temporal variations of extreme climate events

3.1.1. Temporal trends of extreme climate events

Table 1 lists the temporal changes for extreme climate indices in NNRSWC. For NNRHDM, NNRSCB, and NNRYGP, the cold extreme indices for FD0, ID0, TX10p, TN10p and CSDI significantly downtrended by − 4.4 days/10 yr^{-1}, −1.3 days/10 yr^{-1}, and − 1.3 days/10 yr^{-1}; −0.5 days/10 yr^{-1}, −0.1 days/10 yr^{-1}, and − 0.1 days/10 yr^{-1}; −1.8 %/10 yr^{-1}, −0.9 %/10 yr^{-1}, and − 1.2 %/10 yr^{-1}; −4.4 %/10 yr^{-1}, −2.8 %/10 yr^{-1}, and − 3.2 %/10 yr^{-1}; and − 1.0 days/10 yr^{-1}, −0.5 days/10 yr^{-1}, and − 0.9 days/10 yr^{-1}; respectively. However, the cold extreme indices of TXn, TNn and TMINmean in NNRHDM, NNRSCB, and NNRYGP significantly uptrended at rates of 0.3 °C/10 yr^{-1}, 0.2 °C/10 yr^{-1}, and 0.3 °C/10 yr^{-1}; 0.5 °C/10 yr^{-1}, 0.2 °C/10 yr^{-1}, and 0.4 °C/10 yr^{-1}; and 0.3 days /10 yr^{-1}, 0.2 days/10 yr^{-1}, and 0.2 days/10 yr^{-1}, respectively. Abrupt change years occurred in the time range 1986–1997 at 0.01 significance level for all three subregions (Table 1). In NNRHDM, NNRSCB, and NNRYGP, significant uptrends in warm extremes of SU25, TR20, TN90p, TX90p, TXx, TNx, TMAXmean, and WSDI were detected of 3.3 days/10 yr^{-1}, 3.3 days/10 yr^{-1}, and 2.6 days/10 yr^{-1}; 0.9 days/10 yr^{-1}, 2.5 days/10 yr^{-1}, and 3.6 days/10 yr^{-1}; 3.9 %/10 yr^{-1}, 2.4 %/10 yr^{-1}, and 3.3 %/10 yr^{-1}; 3.2 %/10 yr^{-1}, 3.4 %/10 yr^{-1}, and 2.3 %/10 yr^{-1}; 0.3 °C/10 yr^{-1}, 0.4 °C/10 yr^{-1}, and 0.2 °C/10 yr^{-1}; 0.2 °C/10 yr^{-1}, 0.1 °C/10 yr^{-1}, and 0.1 °C/10 yr^{-1}; and 0.3 days/10 yr^{-1}, 0.2 days/10 yr^{-1}, and 0.1 days/10 yr^{-1}, respectively. Abrupt years were detected in 1996 and 1997. Changes in GSL and DTR were also evaluated. The GSL showed a significant uptrend in the NNRHDM (3.8 °C/10 yr^{-1}) and NNRYGP (1.1 °C/10 yr^{-1}), and DTR showed a significant downtrend in NNRYGP (-0.1 °C/10 yr^{-1}). No

Table 1
The trend and abrupt year in Southwest China National Nature Reserve from 1961 to 2019.

Indices	NNRHDM *Sen-slope*	Pettitt	NNRSCB *Sen-slope*	Pettitt	NNRYGP *Sen-slope*	Pettitt
FD0	−0.44**	1986**	−0.13**	1984**	−0.13**	1984**
ID0	−0.05**	1997**	−0.01**	1985**	−0.01**	1985**
TX10P	−0.18**	1997**	−0.12**	1993**	−0.09**	1993**
TN10P	−0.44**	1986**	−0.28**	1993**	−0.32**	1993**
TXn	0.03**	1996**	0.02	1984**	0.02	1984**
TNn	0.05**	1983**	0.02	1984**	0.04**	1984**
CSDI	−0.10**	1978**	−0.05**	1992*	−0.09**	1992*
TMINmean	0.03**	1992**	0.02	1996**	0.02**	1996**
SU25	0.33**	1997**	0.33	1996**	0.26**	1996**
TR20	0.09**	2004**	0.25	1997**	0.36**	1997**
TN90P	0.39**	1992**	0.24	1996**	0.33**	1996**
TX90P	0.32**	1997**	0.34	1996**	0.23**	1996**
TXx	0.03**	2004**	0.04	1993**	0.02**	1993**
TNx	0.02**	1985**	0.01	2000**	0.01**	2000**
TMAXmean	0.03**	1997**	0.02	1996**	0.01**	1996**
WSDI	0.09**	1997**	0.09	1996**	0.09**	1996**
DTR	−0.01	1973**	0.01	1996**	−0.01**	1996**
GSL	0.38**	1995**	0.16	1986**	0.11**	1986**
RX1day	0.07	1978**	0.02	2006	0.05**	2006
RX5day	0.02	1978	−0.15	1984	0.02	1984
R10mm	0.02	1987	−0.04	1985	−0.03	1985
R20mm	0	1982	−0.02	1975	−0.01	1975
R25mm	0.01	1982	−0.01	1975	0	1975
R95p	0.46**	1978**	−0.55	1991	0.38	1991
R99p	0.27**	1988**	−0.06	2006	0.31	2006
CWD	−0.01	2000	−0.02**	2001**	−0.03**	2001**
CDD	0.05	2008	0	1990	0.07	1990
SDII	0.01**	1997**	0	2006	0	2006
PRCPTOT	0.55	1987	−1.47	1985	−0.51	1985

Denote: * Means passing the significance test of 0.05, ** Means passing the significance test of 0.01.

consensus abrupt years for changes in GSL and DTR were identified for the three subregions. During 1961–2019, the extreme precipitation in sub-region change trend and abrupt changes were not obvious. There was uptrend in the NNRHDM, with significant change trends in R95p, R99p, and SDII, as well as abrupt years. There was mainly significant downtrend and abrupt year for CWD in Whilst one extreme precipitation indices displayed an uptrend, eight exhibited a downtrend, and two extreme precipitation indices exhibited no trend in the NNRSCB. Five extreme precipitation indices displayed an uptrend, four exhibited a downtrend, and two extreme precipitation indices exhibited no trend in the NNRYGP. In particular, RX1day (5.0 mm/10 yr^{-1}) showed a significant uptrend and CWD showed a significant downtrend (-0.3 days /10 yr^{-1}).

3.1.2. Spatial distribution of extreme climate events

The spatial distributions of trends for extreme temperature indices are shown in Fig. 2. In the NNRSWC during 1961–2019, there were more stations with negative trends of cold extreme indices for FD0 (90.8 % stations negative, 72.4 % significantly negative), TN10P (98.0 % stations negative, 86.7 % significantly negative), TX10P (89.8 % negative, 46.9 % significantly negative), and CSDI (92.9 % negative trend, 37.8 % significantly negative). A total of 93.9 % stations (67.3 % significantly positive), 86.7 % (52.0 % significantly negative), 95.9 % (82.7 % significantly positive) exhibited positive trends for cold extreme indices of TNn, TXn, and TMINmean, respectively. For ID0 indices, 38.8 % stations showed negative trends (15.3 % were significant, and these stations are mainly distributed in the NNRHDM and NNRSCB) and 52.0 % stations showed no trend in the NNRSWC (mainly distributed in the NNRYGP). The spatial distribution trends for warm extreme indices were also analyzed. More than 85.3 % stations showed positive trends for SU25, TX90P, TN90P, TXx, TNx, TMAXmean, and WSDI, with significantly positive trends for 64.3 %, 82.7 %, 79.6 %, 66.3 %, 68.4 %, 77.6 %, and 33.7 % of total stations, respectively in the NNRSWC. For TR20, 20 % of stations were positive and for WSDI, 2 % of stations showed no trend. For GSL, 84.7 % of stations with positive trends (38.8 % were significantly positive trends), and these were mainly concentrated in NNRHDM and NNRSCB. For DTR, 60.2 % of stations showed negative trends (24.5 % with significant negative trends) and these stations were scattered in the NNRSWC. The FD0, ID0, TX10P, TN10P, SU25, TR20, TN90P, and TX90P change trends showed significant fluctuations in the three subregions (Fig. 2). The fluctuation of abrupt years was also large, with more than 60 % stations significant for extreme temperature indices (Fig. 3), and 90 % stations showing significant abrupt changes for TMAXmean, TMINmean, TX90P, and TN10P indices in the three subregions.

The precipitation indices were evaluated, as show in Fig. 4. Most stations in the NNRSWC have insignificant change trends for extreme precipitation indices other than extreme temperature. Significant uptrends for Rx1day, Rx5day, R95p, R10mm, R20mm, R25m, SDII, CDD, CWD, and PRCPTOT were determined as 8.2 %, 4.1 %, 4.1 %, 4.1 %, 5.1 %, 13.3 %, 12.2 %, 15.3 %, 8.2 %, 0, and 10.2 %, respectively. Significant downtrends for Rx1day, Rx5day, R95p, R10mm, R20mm, R25m, SDII, CDD, CWD, and PRCPTOT were determined as 4.1 %, 5.1 %, 6.1 %, 3.1 %, 2.0 %, 3.1 %, 3.1 %, 2.0 %, 2.1 %, 25.5 %, and 8.2 %, respectively. Significant R1day uptrends were identified for six out of nine stations located in NNRHDM, and significant downtrends for R5day were found for four stations scattered in the NNRSCB and NNRYGP. Stations showing significant uptrends for SDII (11 out of 16 stations), R10 (one of four stations), R20 (all four stations), R25 (five stations), CDD (seven out of eight stations), R95p (eight out of 13 stations), and R99p (nine out of 12 stations) were mainly distributed in the NNRHDM and NNRSCB. For CWD indices, 21 out of 25 stations exhibited significant downtrends, and these were mainly located in the NNRHDP and NNRSCB. The change trend ranges of R95p (Fig. 4i) and PRCPTOT (Fig. 4k) indices show large fluctuations for the three subregions. Compared with the extreme temperature indices (Fig. 2), there were relatively few significant abrupt years of extreme precipitation indices in the three subregions.

3.2. Spatial-temporal and altitudinal changes dynamics variations of NDVI

Spatial distribution of multi-year average NDVI is presented in Fig. 5. In the NNRSWC, the NDVI varied from 0.083 to 0.92, indicating high heterogeneity over the NNRSWC. Maximum NDVI (evergreen broadleaf) was distributed at the southwestern edge of NNRYGP (southwestern of Yunnan) and minimum NDVI (swamp) was located in NNRHDM. The regions with high NDVI values (ranging from 0.8 to 0.9) were mainly distributed in southwestern Yunnan (Nabanhe National Nature Reserve), areas that are covered by evergreen broadleaf. Lower NDVI (0.08–0.4) values were identified in NNRHDM, areas that are covered by swamp and shrub. From 1998 to 2019, high vegetation coverage areas [0.6–0.8) exhibited decreased fluctuation. Maximum vegetation coverage areas [0.8–1.0) increased for three subregions (Fig. 5c-f). After 2007 in the NNRYGP, there was little change in the three subregions with low or lower vegetation coverage.

Fig. 6 shows an increasing trend of NDVI with a rate of 0.00421 yr^{-1} ($R^2 = 0.80$, $p < 0.01$) for NNRHDM, 0.00514 yr^{-1} ($R^2 = 0.85$, $p < 0.01$) for NNRSCB, and 0.00529 yr^{-1} ($R^2 = 0.89$, $p < 0.01$) for NNRYGP (Fig. 6a) during 1998–2019. The distribution of NDVI trends showed spatial heterogeneity, with 79.1 % (69.4 % significant positive trends) of the total areas showing positive trends (greening trend) and 20.9 % (with 13.6 % significantly negative) showing negative trends (browning trend) for NNRHDM. For NNRSCB, 89.9 % (85.5 % significantly

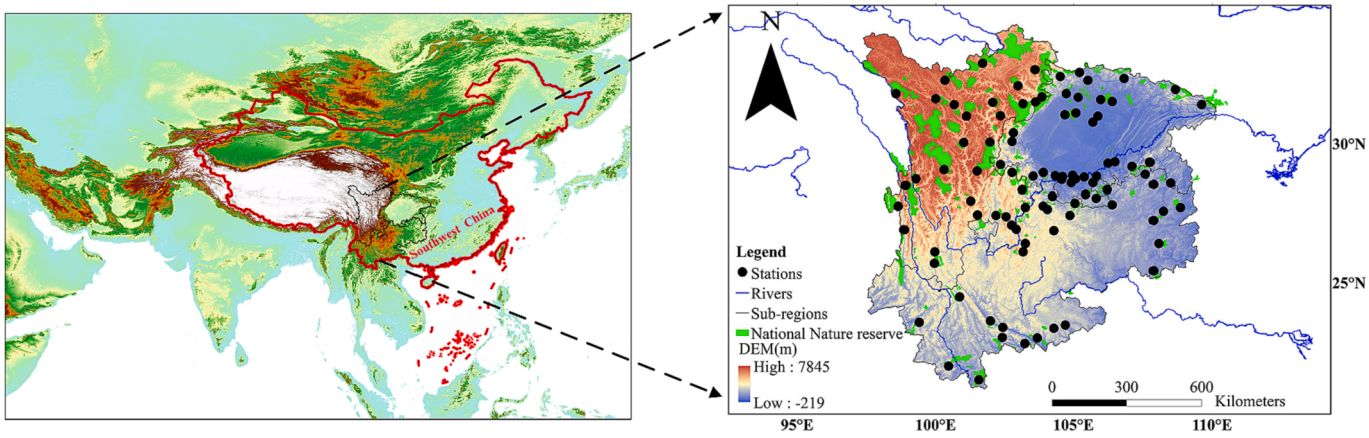

Fig. 1. The geographical location of National Nature Reserves, Southwest China. Mountain range, meteorological station, and Digital Elevation Model (DEM).

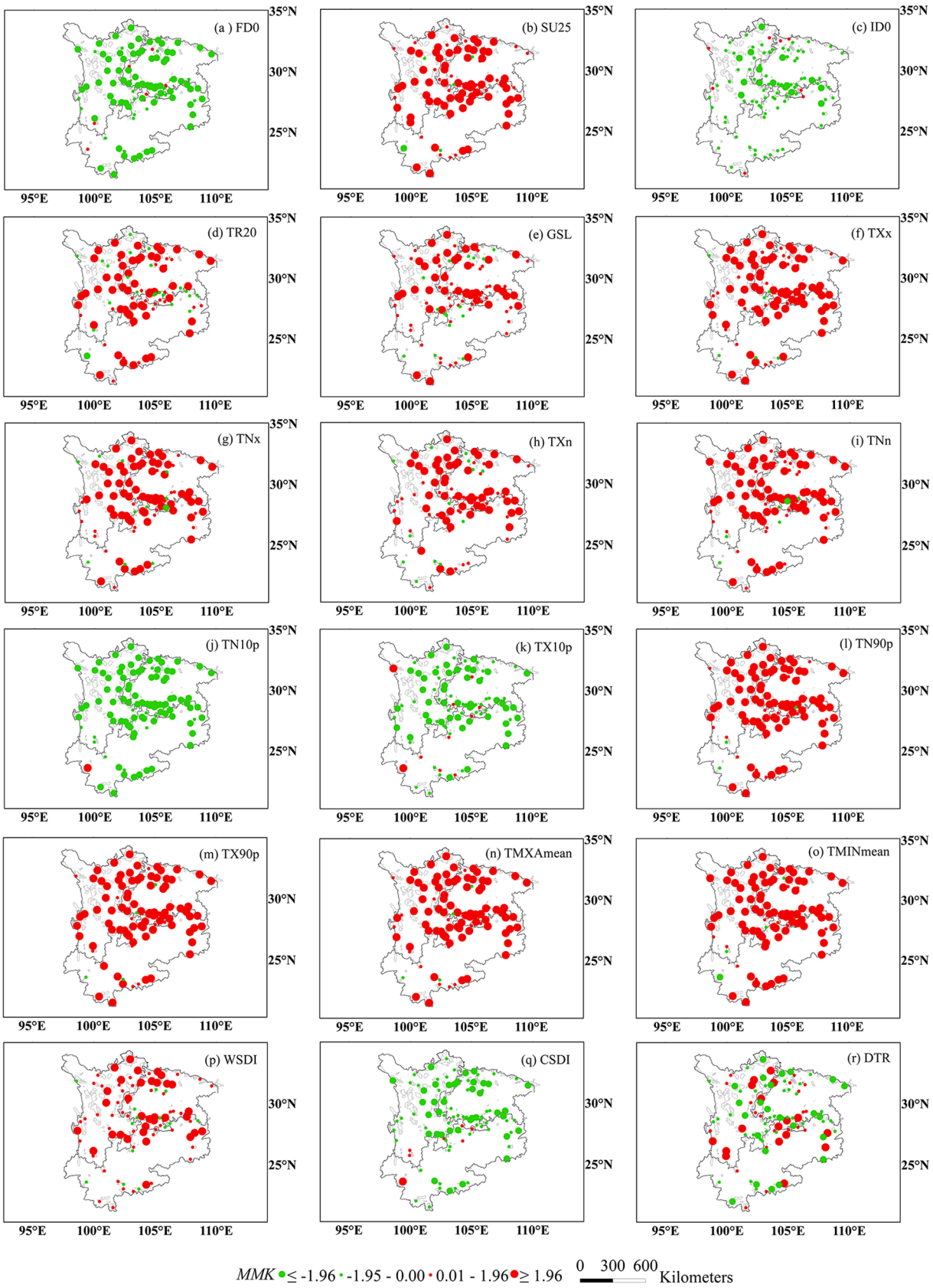

Fig. 2. Spatial distribution of *MMK* values for extreme temperature events during 1961–2019 in Southwest China, National Nature Reserves. *MMK* value greater than 1.96 and *MMK* greater than 2.58 indicate 0.05 and 0.01confidence levels by *MMK* test (consistent with later figures).

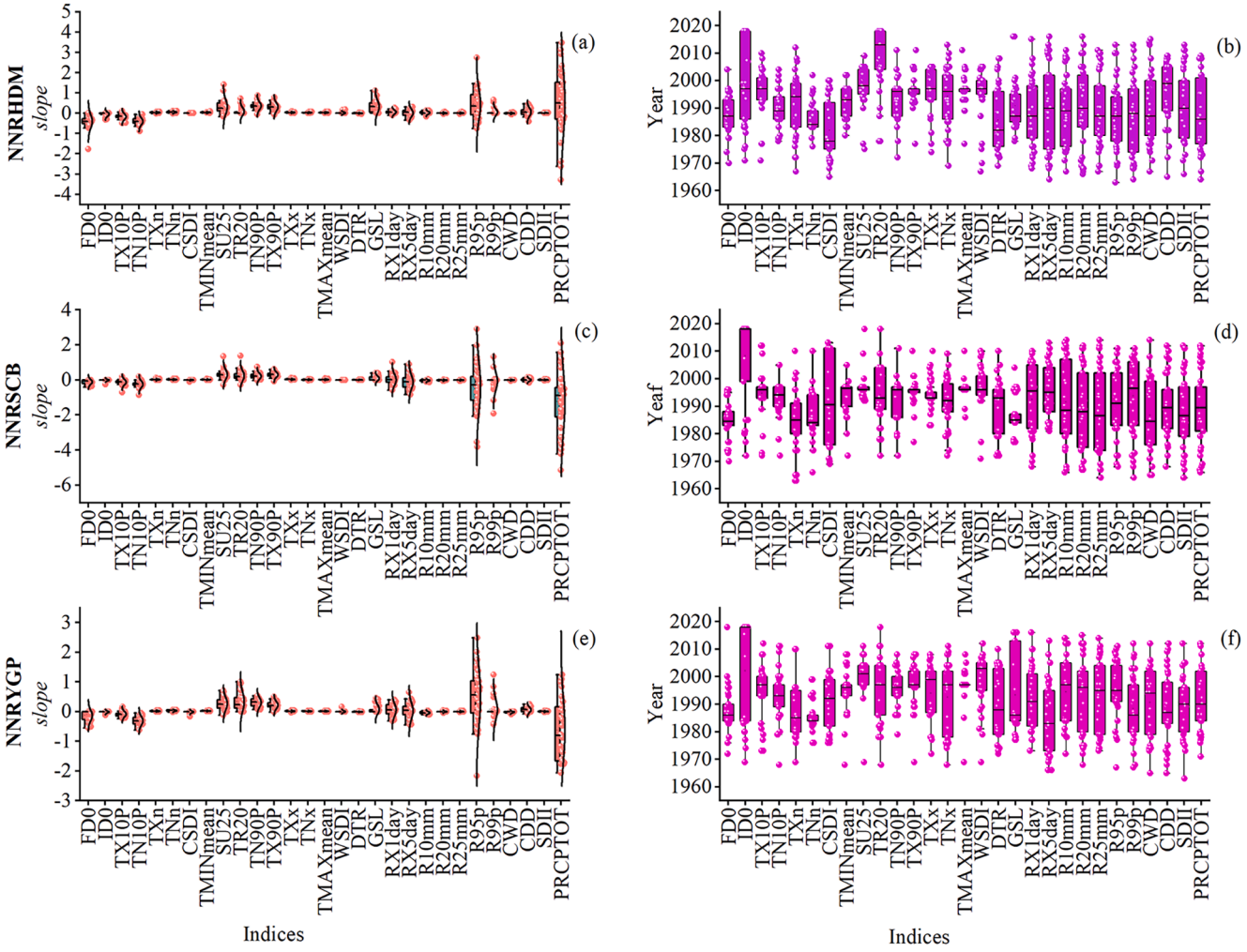

Fig. 3. Extreme temperature and precipitation indices of each station. Sen's slope, abrupt year, and significance percentage values are presented for the National Nature Reserves, Southwest China in the period of 1961–2019.

positive) showed positive trends and 10.1 % (7.0 % significantly negative) showed negative trends. For NNRYGP, 91.6 % (83.9 % significantly positive) showed positive trends and only 8.4 % (3.6 % significantly negative) showed negative trends (Fig. 6b). At monthly timescales, the green trend ranged from 60.1 % (41.7 % significantly increased for January) to 89.3 % (79.2 % significantly increased for October) in the NNRHDM. The monthly NDVI positive trend ranged from 54.8 % (41.0 % significantly increased for June) to 95.3 % (88.7 % significantly increased for October) in the NNRSCB. Monthly NDVI ranged from 55.6 % (32.9 % significantly increased for July) to 99.3 % (97.5 % significantly increased for October) in the NNRYGP, with a significant decreasing (21.7 %) trend detected in July. Overall, the NDVI for the three subregions showed a significant increased trend in October and an obvious seasonal increasing trend in spring (March, April, May).

The elevation bins of annual average NDVI and slope were next analyzed. NDVI values greater than 0.8 were mainly at 1049–2649 m (maximum NDVI value of 0.83 at 1249–1349 m) with corresponding greening trends that ranged from 0.0012 to 0.0058 yr^{-1} at 1049–5649 m (Fig. 7a). A significant change trend was also observed at 1349–2349 m. At the elevation of 5649–6149 m, NDVI tends to browning, and the higher the altitude, the more obvious the fluctuation darkening trend in the NNRHDM. In the NNRHDM, average NDVI values greater than 0.8 were mainly located at 947–2747 m (maximum NDVI value of 0.83 at 1647–1747 m) and the corresponding green trends ranged from 0.0003 to 0.0078 yr^{-1} for 147–4147 m (significant change trend at 847–1447 m (Fig. 7b)). In the NNRYGP, NDVI values greater than 0.8 were mainly found at 617–2817 m (maximum NDVI value of 0.84 for 917–1017 m) with corresponding green trends that ranged from 0.0024 to 0.0087 yr^{-1} for all elevations (and significant change trend at elevation of 217–3017 m (Fig. 7c). Interestingly, the above analysis reveals that the maximum NDVI values and trends are not found in the same altitude zone. Additionally, the green trend was more obvious at lower altitude, and this was more significant in the NNRYGP. Higher altitude zones show darkening trends in the NNRHDM and NNRSCB, but a greening trend in the NNRHDM.

3.3. Correlation analysis for extreme climate indices with NDVI in different buffer areas.

3.3.1. Annual extreme climate indices with NDVI in different buffer areas

Spearman correlation coefficients between annual extreme climate indices and different buffer areas of NDVI were calculated and the results are presented in Table 2. Annual NDVI values were significantly negatively correlated with extreme cold indices of TX10P, TN10P, and CSDI in different buffer areas. Extreme warm indices of TR20, TXx, and TNx showed significantly positive correlation in the NNRHDM and NNRYGP (for 5 km and 10 km) in different buffer areas, with higher correlation coefficients for 10 km. The annual average NDVI was not significantly correlated with extreme temperature for WSDI, DTR, and GSL in the three subregions. Additionally, there was no significant correlation for almost all extreme precipitation indices in the three subregions (except in the NNRHDM for some indices). Overall, the

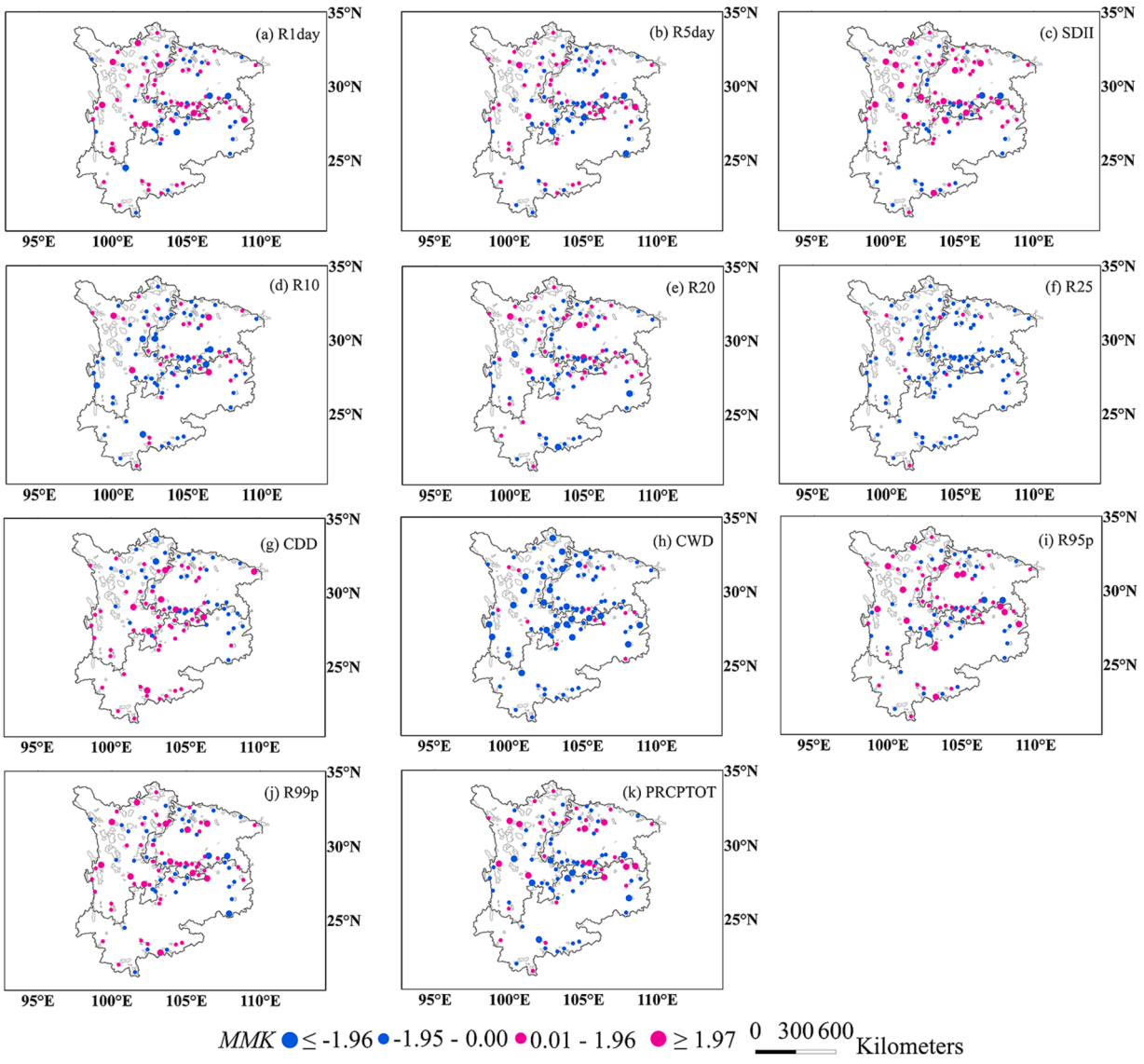

Fig. 4. Spatial distribution of *MMK* values for extreme precipitation events over 1961–2019 in Southwest China, National Nature Reserves.

correlation of extreme temperature indices with annual NDVI for different buffer areas (correlation value higher in 10 km) was more significant in the three subregions. In the NNRHDM, extreme temperature and precipitation were more significantly correlated than in the NNRSCB and NNRYGP.

The relationships between annual average NDVI and extreme climate indices were determined for each station and the results are shown in Fig. 8. In the 2 km and 5 km buffer areas, the positive and negative significance correlations are scattered, with no consistent characteristic in three subregions. There was significant negative correlation in the NNRHDM and positive correlation with cold extreme indices in the NNRSCB and NNRYGP for a 10 km buffer area. In the 2 km buffer area, there were significant positive correlation with warm indices for SU25, TR20, TX90P, TN90P, TXx, TNx, and TMAXmean with 9.1 %/2.9 %/6.5 %, 12.1 %/2.9 %/16.1 %, 9.1 %/5.9 %/9.7 %, 3.0 %/2.9 %/16.1 %, 21.2 %/5.9 %/9.7 %, 18.2 %/11.8 %/22.6, and 18.2 %/0/9.7 % respectively for NNRHDM/NNRSCB/NNRYGP (statistics based on the total number of stations in the three subregions). There were significant positive correlations with extreme precipitation for R10, R20, R25, R95, R99, CDD, CWD, SDII, PRCPTOT of 6.1 %/8.8 %, 12.1 %/5.9 %, 3.0 %/5.9 %, 6.1 %/5.9 %, 6.1 %/0, 6.1 %/0, 12.1 %/0, 9.1 %/11.8, and 12.1 %/8.8 %, respectively, in the NNRHDM/NNRSCB. For the 5 km buffer areas, the correlations between NDVI and extreme warm indices (SU25, TR20, TX90P, TN90P, TNx, TXx, and TMAXmean) exhibited significant positive correlations for 24.2 %/0/12.9 %, 9.1 %/2.9 %/32.3.8 %, 18.2 %/8.8 %/19.4 %, 15.2 %/5.9 %/32.3 %, 42.4 %/14.7 %/22.6 %, 27.3 %/11.8 %/32.3 %, and 42.4 %/5.9 %/16.1 %, respectively, in the NNRHDM/NNRSCB/NNRYGP. There were also significant positive correlations with extreme precipitation for RX1day (12.1 %/2.9 %), RX5day (12.1 %/2.9 %), R10 (9.1 %/8.8 %), R20 (9.1 %/2.9 %), R25 (15.2 %/5.9 %), R95 (12.1 %/2.9 %), R99 (12.1 %/0), CDD (6.1 %/0), CWD (15.2 %/2.9 %), SDII (15.2 %/2.9 %), PRCPTOT (18.2 %/11.8 %), respectively, in the NNRHDM/NNRSCB. For the 10 km buffer area, 39.4 %/2.9 %/16.1 %, 12.1 %/2.9 %/54.8 %, 21.2 %/5.9 %/25.8 %, 15.2 %/2.9 %/38.7 %, 36.4 %/20.6 %/25.8 %, 30.3 %/14.7 %/41.9 %, and 45.5 %/8.8 %/32.3 % of the total stations showed positive correlations for warm indices (SU25, TR20, TX90P, TN90P, TXx, TNx, and TMAXmean), respectively, in the NNRHDM/NNRSCB/NNRYGP. There was also significant positive correlation between extreme precipitation indices and annual average NDVI in the NNRSCB and NNRYGP. Overall, the extreme cold (negative) and warm (positive) temperature indices were more obviously significantly correlated in the three subregions than extreme precipitation, with more significant impact on annual average NDVI for different buffer areas (except in 10

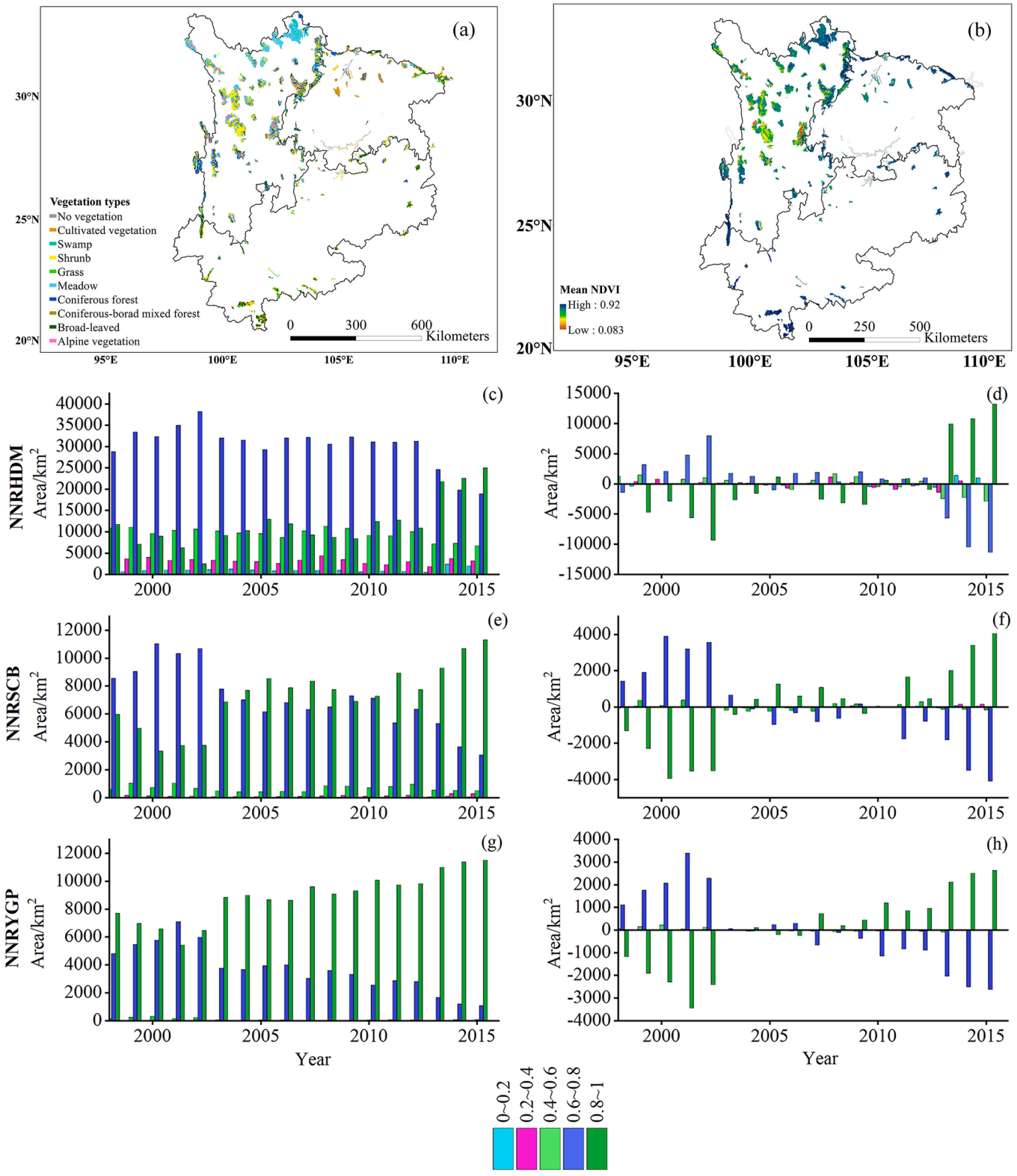

Fig. 5. Vegetation type for the National Nature Reserves, Southwest China, for 1998–2019. (a), multi-year average NDVI (b), annual NDVI dynamic changes (c, e, g) and anomaly (d, f, h) for three sub-regions in 1998–2019. Vegetation NDVI was classified using an equal-interval method and the actual status of vegetation NDVI: 0 < 0.2, low vegetation coverage; 0.2–0.4, lower vegetation coverage; 0.4–0.6, moderate vegetation coverage; 0.6–0.8, high vegetation coverage; 0.8–1, maximum vegetation coverage.

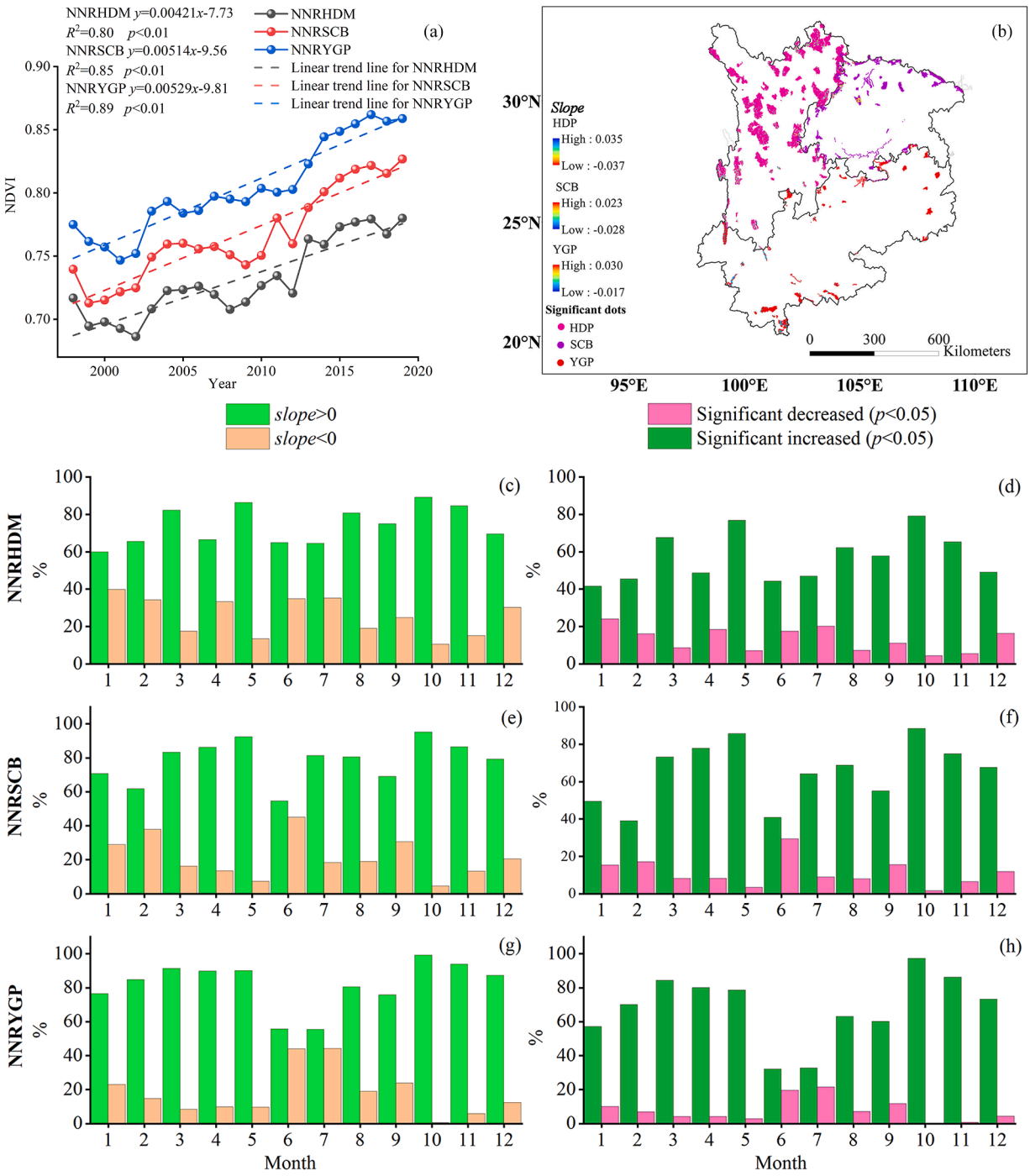

Fig. 6. Temporal (a) and spatial trends (b) of NDVI, change percentages of slope greater than 0 and < 0 (c, e, g) and significant increase and decreased (d, f, h) for three sub-regions of the National Nature Reserves, Southwest China over the period of 1998–2019.

km areas for the NNRSCB and NNRYGP).

3.3.2. Monthly extreme climate indices with NDVI in different buffer area

As shown in Figs. 9-10, more than 70 % of stations show significant positive correlation of the extreme climate indices (TNn, TNx, TXn, TXx, TMAXmean, TMINmean, RX1day, RX5day) with different buffer areas of NDVI for lag 0 month in the NNRHDM/NNRYGP. For lag 3–6 month, more than 70 % of stations manifest significant negative correlation, especially for lag 3–5 month for different buffer areas in the NNRHDM and NNRYGP. Furthermore, for almost all stations, the extreme climate indices (TNn, TNx, TXn, TXx, TMAXmean, TMINmean, RX1day, and RX5day) show significant positive correlation in lag 0–2 month and significant negative correlation in lag 4–6 month with different buffer areas of NDVI in the NNRSCB. However, for TX10P, TN10P, TX90P, TN90P indices, the significant positive and negative proportions are relatively small with different buffer areas of NDVI for lag 0–6 month in the three subregions.

According to the above analysis, the correlation between extreme climate indices with NDVI in different buffer areas gradually showed significant positive correlation with a lag of 0–1 months and reached significant negative correlation with a lag of 3–6 months, especially in the NNRHDM and NNRYGP. However, in the NNRSCB, the significant positive correlation with a lag of 0–2 months gradually changed to a significant negative correlation with a lag of 3–6 months.

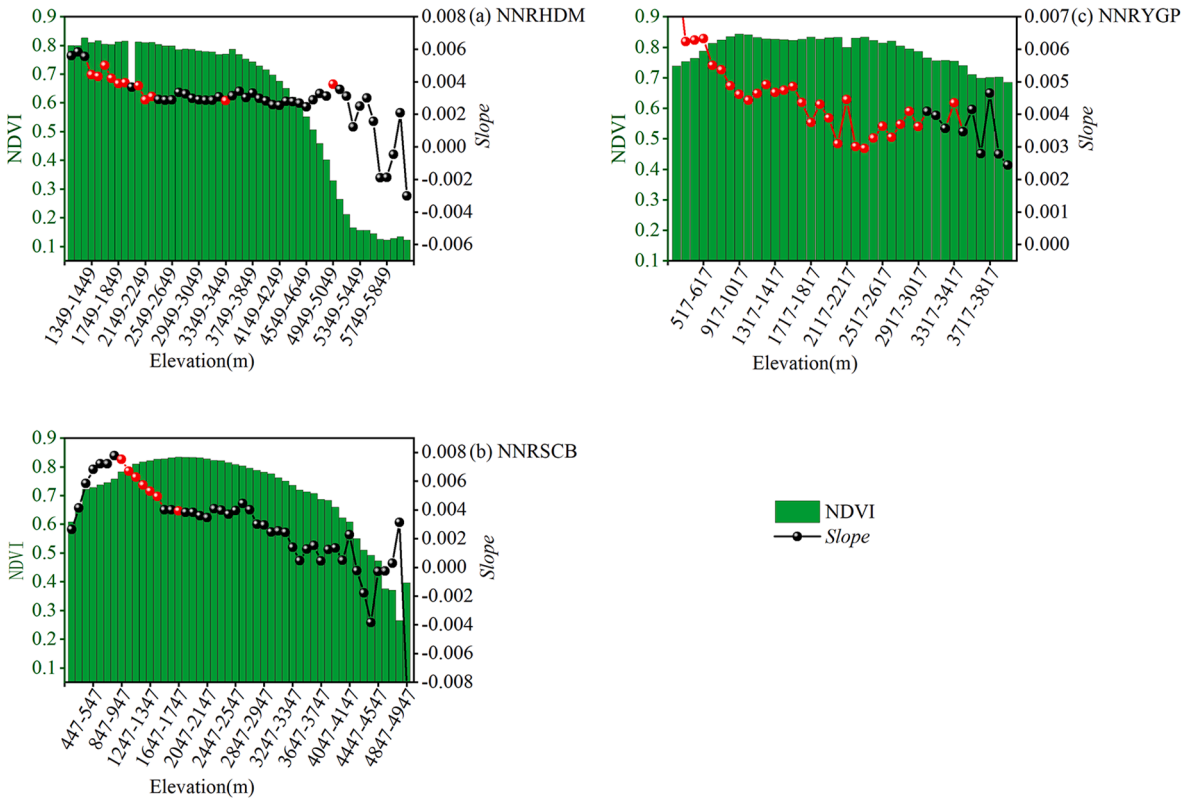

Fig. 7. Annual average NDVI (column bar) and slope (line with symbol) during 1998–2018 for each elevation bin in the National Nature Reserves, Southwest China (red dots indicate *MMK* value greater than 1.96 at 0.05 significant confidence level for slope). (For interpretation of the references to color in this figure legend, the reader is referred to the web version of this article.)

Table 2
Correlation coefficients between extreme climate indices with annual average NDVI for different buffer areas in the NNRSWC from 1998 to 2019.

	NNRHDM			NNRSCB			NNRYGP		
Indices	NDVI2	NDVI5	NDVI10	NDVI2	NDVI5	NDVI10	NDVI2	NDVI5	NDVI10
FD0	−0.10	−0.33	−0.40	0.05	−0.13	−0.10	−0.14	−0.33	−0.29
ID0	−0.46*	−0.55**	−0.54*	0.06	−0.08	−0.04	0.01	−0.08	−0.03
TX10P	−0.51*	−0.67**	−0.69**	0.18	−0.13	−0.18	−0.11	−0.51*	−0.47*
TN10P	−0.46*	−0.62**	−0.64**	−0.11	−0.38	−0.39	−0.27	−0.74**	−0.76**
TXn	0.07	0.12	0.14	0.15	0.13	0.07	0.05	0.01	−0.06
TNn	0.02	0.12	0.13	−0.25	−0.04	0.01	0.11	0.17	0.13
CSDI	−0.30	−0.39	−0.32	−0.19	−0.51*	−0.46*	−0.49*	−0.62**	−0.58**
TMAXmean	0.56**	0.63**	0.66**	0.07	0.13	0.17	0.13	0.41	0.39
SU25	0.11	0.15	0.21	−0.06	−0.09	0.00	0.08	0.37	0.39
TR20	0.66**	0.64**	0.69**	0.32	0.33	0.32	0.12	0.68**	0.69**
TN90P	0.25	0.427*	0.46*	0.01	0.03	0.09	0.30	0.57**	0.54*
TX90P	0.29	0.38	0.42	0.22	0.15	0.15	0.29	0.42	0.39
TXx	0.53*	0.71**	0.76**	0.23	0.37	0.34	0.23	0.53*	0.52*
TNx	0.51*	0.72**	0.73**	0.38	0.30	0.22	0.08	0.48*	0.60*
TMINmean	0.36	0.62**	0.66**	0.03	0.14	0.18	0.18	0.73**	0.73**
WSDI	0.20	0.35	0.40	0.03	0.03	0.06	0.19	0.38	0.39
DTR	0.05	0.15	0.13	0.06	0.01	0.06	0.02	−0.20	−0.23
GSL	0.09	0.39	0.36	−0.07	0.08	0.08	0.03	0.06	−0.01
RX1day	0.19	0.32	0.36	0.23	0.31	0.24	−0.06	0.29	0.30
RX5day	0.42	0.55**	0.62**	0.24	0.29	0.24	0.01	0.17	0.11
R10	0.05	0.16	0.14	0.09	0.43*	0.48*	−0.02	0.15	0.17
R20	0.02	0.10	0.11	−0.02	0.33	0.42	0.01	0.15	0.13
R25	−0.05	−0.04	−0.03	0.07	0.32	0.39	−0.01	0.21	0.17
R95p	0.42	0.49*	0.51*	0.10	0.26	0.29	0.07	0.21	0.19
R99p	0.37	0.47*	0.52*	0.30	0.35	0.29	−0.03	0.33	0.32
CWD	0.14	0.23	0.24	−0.26	−0.02	0.00	−0.25	−0.13	−0.15
CDD	0.44*	0.26	0.25	−0.03	−0.13	−0.15	0.20	0.03	0.07
SDII	0.38	0.56**	0.61**	0.20	0.26	0.29	0.05	0.25	0.22
PRCPTOT	0.11	0.15	0.15	0.10	0.44*	0.48*	−0.06	0.17	0.16

Denote: * means passing the significance test of 0.05,** means passing the significance test of 0.01.

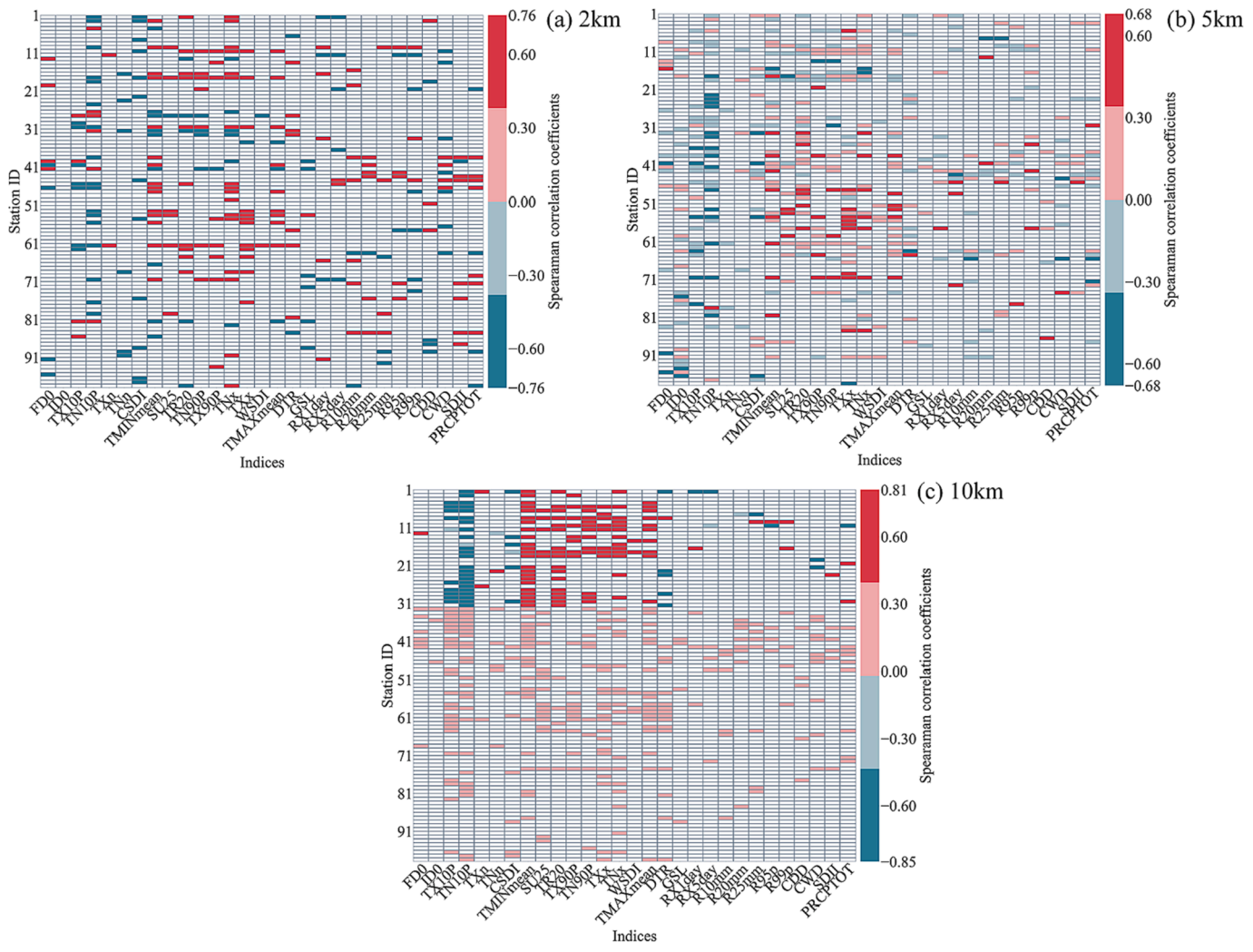

Fig. 8. Spearman correlation coefficients for extreme climate indices with different buffer area of annual NDVI over the 1998–2019 in the National Nature Reserves, Southwest China. Station ID 1–33 denotes NNRHDM, station ID 34–67 denotes NNRSCB, and station ID 68–98 denotes NNRYGP. Color indicates the significance level of 0.05, blank area indicates that the correlation is not significant.

3.4. Multiple stepwise regression reveals the impact of extreme climate on NDVI

We further used multiple stepwise linear regression to assess the ability of different extreme indices to interpret NDVI change. As shown in Table 3, at the annual scale, in the NNRHDM, a combination of RX1day and TNx explain 63 % ($p < 0.05$) of NDVI change in the 10 km buffer area. In the NNRSCB, NDVI in the 10 km buffer area can be explained (47 %) by a combination of R10mm, TN10P, and TXx ($p < 0.05$). In the NNRYGP, FD0, ID0, CSDI, TMINmean, TR20, and WSDI explain 92 % ($p < 0.05$) of NDVI change in the 5 km buffer area. On a monthly timescale, extreme climate indices are even more explanatory. In the NNRHDM, DTR, RX5day, TN10P, TN90P, TNn, TNx, TX90P, and TXx explain 82 % ($p < 0.05$) of NDVI change in the 2 km buffer area. In the NNRSCB, DTR, TMAXmean, TN10P, TN90P, TNn, TX10P, and TX90P explain 80 % ($p < 0.05$) of NDVI change in the 2 km buffer area. In the NNRYGP, a combination of DTR, TMINmean, TN10P, TN90P, TNn, TX90P, TXn, and TXx explain 83 % ($p < 0.05$) of NDVI change in the 2 km buffer area.

4. Discussion

4.1. Change trends of NDVI

Previous studies have reported the characteristics and trend of NDVI change in SWC. However, to the best of our knowledge, no studies have focused on NNRSWC. In this study, our results show that NDVI from 0.8 to 1 tends to fluctuate and increase and NDVI from 0.6 to 0.8 tends to fluctuate and decrease for NNRSCB and NNRYGP during 1998–2019. The results are consistent with previous findings (Peng et al., 2019). The three subregions exhibited green trends (0.00421 yr^{-1} for NNRHDM, 0.00514 yr^{-1} for NNRSCB and 0.00529 yr^{-1} for NNRYGP), in agreement with previous SWC studies (Sun et al., 2022; Tao et al., 2018; Yan et al., 2021) and similar to measurement for the Qilian Mountain Nature Reserve (0.003–0.004 yr^{-1}) in Northwest China (Gao et al., 2021; Ma et al., 2022) and Wuyi Mountains National Nature Reserve (0.0048 yr^{-1}) in Fujian Province, China (Li et al., 2021). Analysis of the different elevation bins shows NDVI values greater than 0.8 mainly concentrated at 1049–2349 m, 947–2547 m, and 617–2817 m in the NNRHDM, NNRSCB, and NNRYGP, respectively. These values for NNRSCB and NNRYGP are relatively close to previously reported values from Peng et al. (2019) for Sichuan province and Huo and Sun (2021) for northwest Yunnan Plateau. The NDVI trends decreased greater than 5649 m in the NNRHDM and greater than 4147 m in the NNRSCB, but NDVI trends

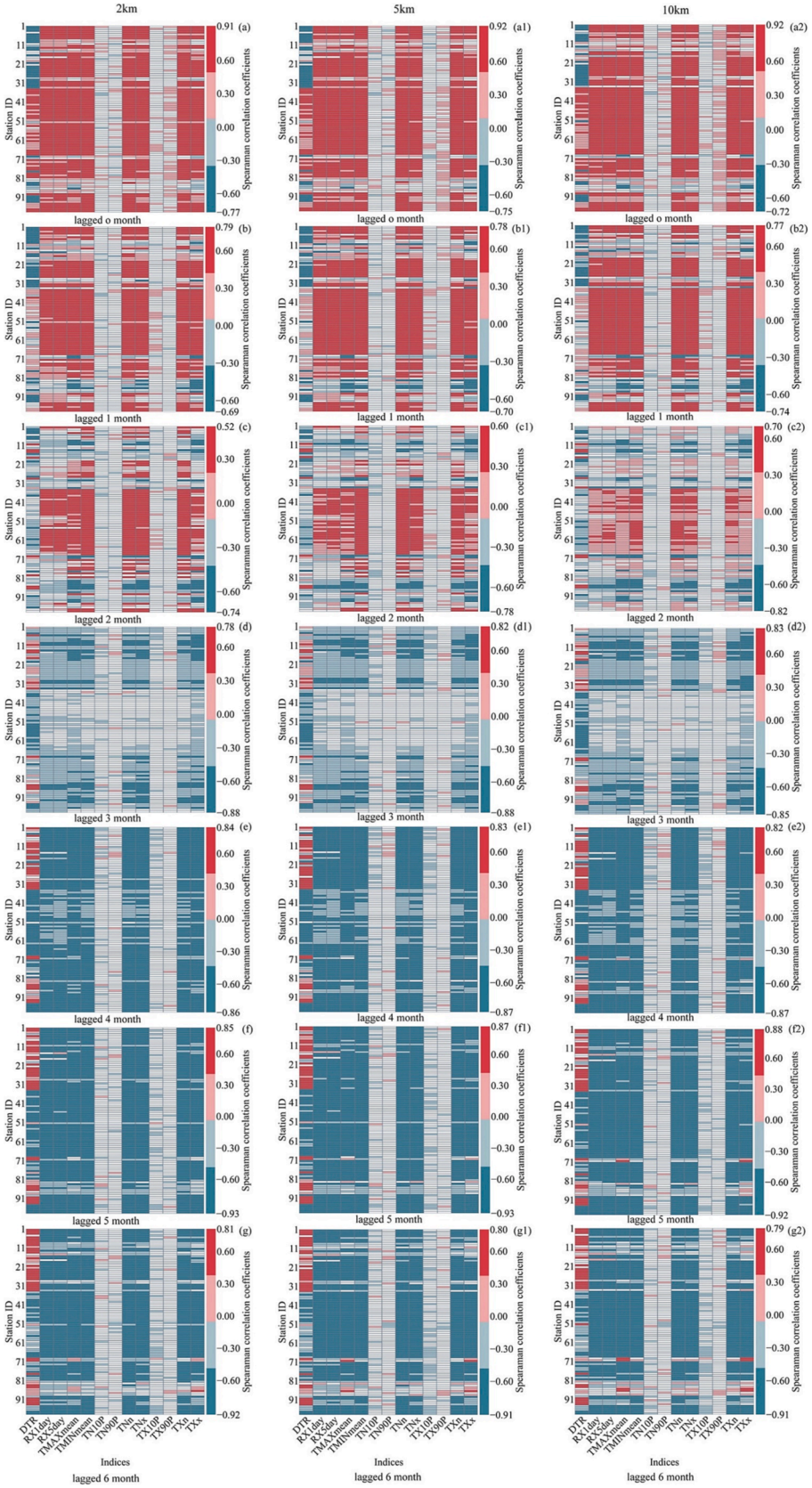

Fig. 9. Correlation of monthly extreme climate indices between NDVI with lag of 0–6 months in the National Nature Reserves, Southwest China. Station ID 1–33 denotes NNRHDM, station ID 34–67 denotes NNRSCB, and station ID 68–98 denotes NNRYGP. Color indicates a significance level of 0.05 and a blank area indicates no significant correlation.

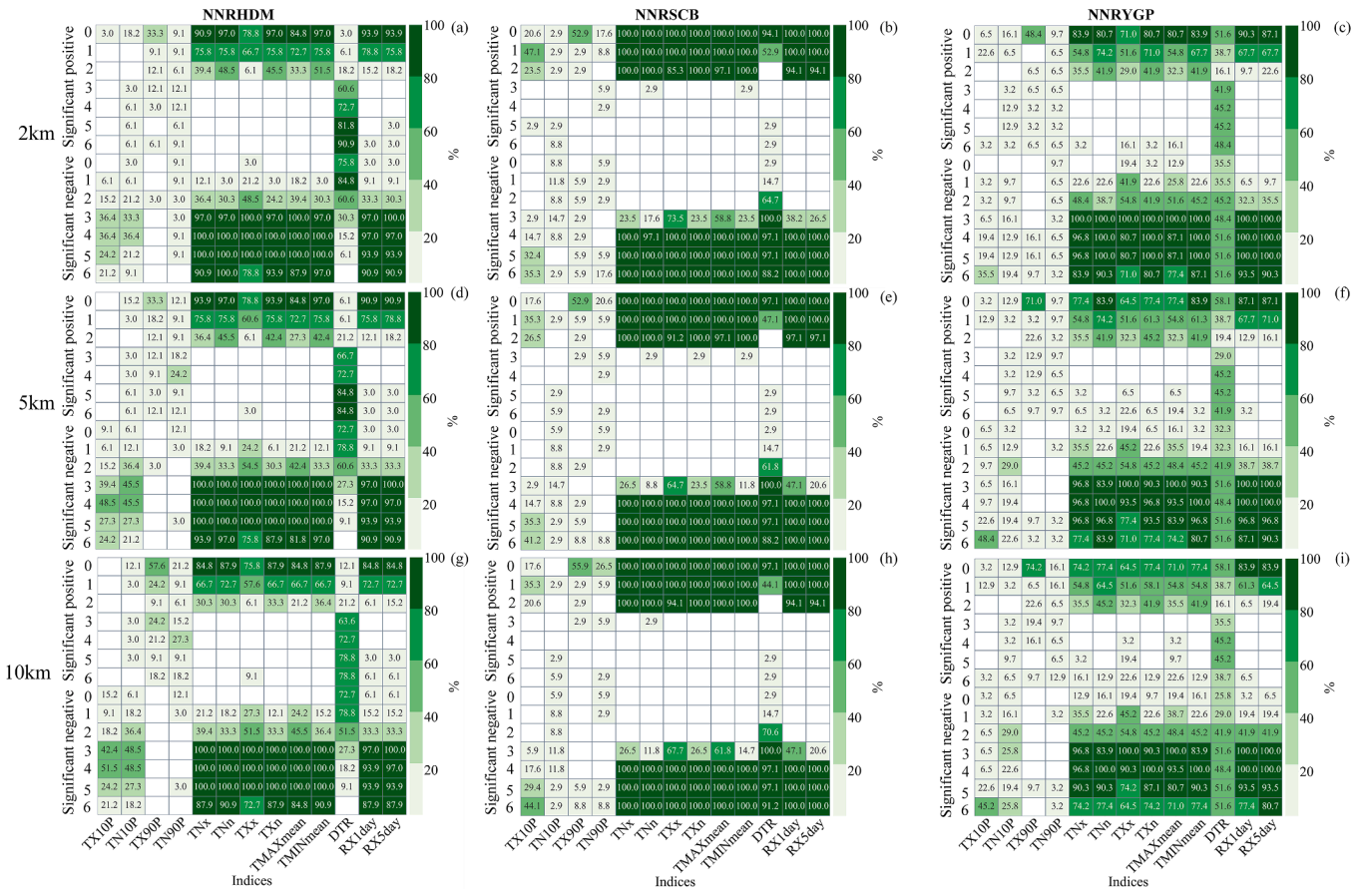

Fig. 10. Spearman correlation coefficient of significant percentages for monthly extreme climate events with different buffer areas of NDVI with a lag of 0–6 months in the National Nature Reserves, Southwest China.

increased in whole elevation bins in the NNRYGP. These results are inconsistent with previously reported decreased trends for 3400–3500 m, with these areas suggested to be unsuitable for vegetation greening (Huo and Sun, 2021; Jiang et al., 2021a; Tao et al., 2018). The different results likely are due to the analysis of the whole NDVI of SWC, with different resolution of NDVI and DEM. Different regional climatic characteristics, study scopes, periods, and selected variables can result in different NDVI trends (Hao et al., 2021; Huo and Sun, 2021). The NDVI green trend was more significant in the low elevation bins for the three subregions, with the trend consistent with that observed for the Wuyi Mountains National Nature Reserve in Fujian Province, China (Li et al., 2021). NDVI dynamics are seldom limited by energy or water in low elevation bins (Jiang et al., 2021a). Overall, we found decreasing average NDVI trend with increasing elevation in the three subregions (though the change trend decreases with increased elevation, the elevation bins still show a positive trend in the NNRYGP).

4.2. *Effects of extreme climate indices on NDVI in different buffer zones*

Climate change and natural factors exert obvious and significant effects on vegetation dynamics that exceed those of human activities in SWC and Tibetan Plateau China (Li et al., 2016; Huo and Sun, 2021; Jiang et al., 2021b; Li et al., 2018a; Liu et al., 2018, 2020; Ma et al., 2021; Tao et al., 2018; Yan et al., 2021). Temperature was the dominant climatic factor impacting NDVI dynamics in the SWC (Ma et al., 2021; Yan et al., 2021) but there are significant seasonal (Ma et al., 2021) and elevation-dependent (Ma et al., 2022; Tao et al., 2018) effects. Additionally, NDVI dynamics also exhibit obvious spatial heterogeneity. For example, vegetation changes in the northeastern and southwestern Tibetan Plateau are water-limited, the mid-eastern Tibetan Plateau exhibits strong temperature responses, and the southern part of the Tibetan Plateau is influenced by temperature and solar radiation (Li et al., 2018a). The role of precipitation was higher than that of temperature in the interaction between NDVI and climatic factors in the Red River Basin (Gu et al., 2018). Solar radiation is also an important meteorological factor in the SWC (Yan et al., 2021). Other important natural factors can limit vegetation change. The precipitation of the driest month significantly affected the extent of vegetation greening in the SWC (20.64 %) (Liu et al., 2020). In the northwestern Yunnan Plateau, soil type, elevation, geomorphic type, and vegetation type explain 24.8 %, 18.6 %, 16.1 %, and 13.2 % of fractional vegetation cover in northwestern Yunnan Plateau (Huo and Sun, 2021). Soil types, elevation, and annual mean temperature satisfactorily explain vegetation changes in Sichuan province (Peng et al., 2019).

Natural factors can also have synergistic effects that exceed the influences of individual factors (Huo and Sun, 2021; Liu et al., 2020; Peng et al., 2019). Although the above studies focused on average meteorological and natural factors, they did not address the potential impacts of extreme climate indices on NDVI dynamics. Here, our results indicated that extreme temperature indices can have more significant influence than extreme precipitation indices, a finding that is consistent with that of some previous studies (Li et al., 2018a,b; Tan et al., 2015). Li et al. (2016) studied Yarlung Zangbo Grand Canyon Nature Reserve and Gao et al. (2021) and Ma et al. (2022) studied the Qilian Mountains (Nature Reserve) in Northwest China and also found that compared with precipitation, temperature has a more significant promotion effect on vegetation growth. From the perspective of the impact of extreme climate on NDVI, we conclude that the impact of extreme temperature indices on NDVI is more significant than that of extreme precipitation. This may be because the climate is controlled alternately by the South

Table 3
Multiple stepwise linear regression between extreme climate indices and NDVI for different areas on annual and monthly scales during 1998–2019.

Timescales	Region	Extreme climate combination	R^2	Adj-R^2	p
	NNRHDM-2 km				
	NNRHDM-5 km	RX1day-TNx	0.62	0.58	0.05
	NNRHDM-10 km	RX1day-TNx	0.67	0.63	0.05
Year	NNRSCB-2 km				
	NNRSCB-5 km				
	NNRSCB-10 km	R10mm-TN10P-TXx	0.55	0.47	0.05
	NNRYGP-2 km	CSDI-DTR-FD0-ID0	0.7	0.63	0.05
	NNRYGP-5 km	CSDI-FD0-ID0-TMINmean-TR20-WSDI	0.95	0.92	0.05
	NNRYGP-10 km	CSDI-ID0-SU25-TMINmean-WSDI	0.94	0.91	0.05
	NNRHDM-2 km	DTR-RX5day-TN10P-TN90P-TNn-TNx-TX90P-TXx	0.81	0.82	0.05
	NNRHDM-5 km	DTR-RX1day-TN90P-TNn-TNx-TX90P-TXx	0.79	0.8	0.05
	NNRHDM-10 km	RX1day-TNn-TNx-TX90P-TXx	0.72	0.73	0.05
	NNRSCB-2 km	DTR-TMAXmean-TN10P-TN90P-TNn-TX10P-TX90P	0.79	0.8	0.05
Month	NNRSCB-5 km	DTR-TMINmean-TN10P-TN90P-TNn-TX10P-TX90P	0.75	0.75	0.05
	NNRSCB-10 km	DTR-TMINmean-TN10P-TN90P-TX10P-TX90P	0.7	0.71	0.05
	NNRYGP-2 km	DTR-TMINmean-TN10P-TN90P-TNn-TX90P-TXn-TXx	0.82	0.83	0.05
	NNRYGP-5 km	DTR-TMINmean-TN10P-TN90P-TNn-TX90P-TXx	0.79	0.8	0.05
	NNRYGP-10 km	DTR-TMINmean-TN90P-TNn-TX90P-TXx	0.74	0.76	0.05

Denote: blank means no significance test has been used.

Asia monsoon and the East Asian monsoon in SWC, bringing abundant precipitation, so these areas are seldom limited by water and more affected by extreme temperature impacts. A separate study used multivariate regression analysis and found climate change explained 54.1 % of changes in vegetation dynamics in the SWC based on multiple time scale analysis (Liu et al., 2018). Li et al. (2018a) suggested that the impact of anthropogenic activities on vegetation change might be less than that of climate change on the Tibetan Plateau. Liu et al (2020) found that climate change, human activities, and topography respectively explain 42.65 %, 33.16 %, and 16.48 % of vegetation change in the SWC. Huo and Sun (2021) determined that vegetation dynamics were primarily driven by soil type (24.8 %), elevation (18.6 %), geomorphic type (16.1 %), vegetation type (13.2 %), and anthropogenic factors (10 %) in northwestern Yunnan Plateau, with only weak effects of mean annual temperature, precipitation, and sunshine duration. The relationship is likely weaker for extreme precipitation indices than that for extreme temperature indices in subtropical areas with abundant annual precipitation. Our study area is a National Nature Reserve, so obviously, the impact of human activities is negligible and the main driving factors of NDVI change are climate and natural factors. At the monthly scale, multiple extreme climates can better explain the changes in NDVI for NNRSCB and NNRGYGP, while the combination of multiple extreme temperature and precipitation indices can better explain the NDVI of NNRHDM. Overall, the trend of NDVI changes is more pronounced in NNRGYGP than in NNRHDM and NNRSCB, with greater sensitivity to extreme temperature responses. Natural factors for soil type, elevation, geomorphic type and vegetation type do not change dramatically over a short period of time, and vegetation responses to climate change may have significant time-lag effects, which may better predict vegetation dynamics under climate change (Wu et al., 2015). For example, climatic factors explained 64 % variation of the global vegetation growth, 11 % higher than the amount explained by the model when time-lag effects were ignored (Wu et al., 2015). Gu et al. (2018) also found a time lag effect between the NDVI response to precipitation and temperature variations in the Red River basin. NDVI also showed significant lagged correlation with extreme climate indices in different buffer area in other studies (Gu et al., 2018; Wu et al., 2015). The trend changed gradually from a significant positive lagged correlation with a lag of 0–2 months to a significant negative correlation with a lag of 3–6 months, especially in the NNRHDM and NNRYGP. Overall, our results suggest that extreme climate indices more strongly explain the NDVI change in the NNRHDM and NNRYGP at annual and monthly scales, especially in the NNRYGP. However, the extraction of NDVI from different buffer zones around the station may affect correlations between NDVI and extreme climate indices and the overall interpretation of NDVI change.

4.3. Limitations and future work

Vegetation dynamics are complex and are related to multiple natural and human factors. There are some limitations and uncertainties of our conclusions. The National Nature Reserve, especially the core area, experiences little human activities, and there are almost no stations in the nature reserve (for example, Yunnan Province has only one station in Ailaoshan National Nature Reserve). These data have long timescales, and although there are now some automatic weather stations, only incomplete data are available for short periods of time, so data from meteorological stations close to the nature reserve must be used to extract the NDVI values for 2 km, 5 km and 10 km areas, potentially leading to uncertainty in the results. Additionally, our study did not consider potential impacts of soil type, elevation, geomorphic type, and vegetation type, which may lead to over-interpretation of extreme climate indices. However, although altitude, landform and vegetation types can significantly impact NDVI, these elements are fixed for a relatively long time. Future work could include analysis of multiple time scales, which might further elucidate the mechanisms of vegetation dynamics (Liu et al., 2018). NDVI with different resolutions may also affect the results. For example, Ma et al. (2021) reported that karst NDVI prediction was better at a spatial resolution of 1 km than at spatial resolutions of 250 m or 8 km. Additionally, related research revealed bioclimatic variables were more suitable than raw climatic factors to examine the relationship between climate changes and vegetation greening (Liu et al., 2018). Many questions remain. Are the current number and spatial distribution of protected areas adequate (Wu et al., 2023)? What are the impacts of protected areas on nearby towns and cities (Naidoo et al., 2019)? Can protected areas serve as refuges for biodiversity with increased climate change (Xu et al., 2022)? How effectively are reserve areas protected (Shrestha et al., 2021)? How do species within protected areas adapt to continuous climate change and human activities? How should climate change be effectively monitored in protected areas? Is adjustment required for existing functional areas (experimental areas, buffer areas and core areas)? Answering these critical questions is required to effectively respond to climate change and better protect biodiversity and maintain ecological functions. However, addressing these issues requires long-term and in-depth research. In this study, we focused on NDVI changes in NNRSWC to assess the impacts of climate change on NDVI in protected areas. In the future, we will extend this work to provide scientific reference to protect biodiversity and facilitate the construction of more effective protected areas.

5. Conclusions

Comprehensive understanding of the relationship between climate extremes and vegetation may help evaluate the resilience and vulnerability of vegetation to climate extremes (Tan et al., 2015), which could facilitate adaptation to and mitigation of climate extremes. In this study, we investigated the change trends of vegetation greenness and extreme climate in the National Nature Reserves of Southwest China and explored the driving effects of extreme climate on vegetation greenness. The main conclusions are as follows:

(1) The average NDVI exhibited a large fluctuation that varied from 0.083 to 0.92. This indicated high heterogeneity over the NNRSWC. Effects on the 1049–2349 m, 947–2547 m, 617–2817 m were, respectively, 0.00421 $year^{-1}$, 0.00514 $year^{-1}$, and 0.00529 $year^{-1}$ in the NNRHDM, NNRSCB, and NNRYGP.
(2) Extreme cold indices (FD0, ID0, TX10p, TN10p, TXn, TNn, and TMINmean) significantly decreased and extreme warm indices (SU25, TR20, TN90p, TX90p, TXx, TNx, TMAXmean, and WSDI) significantly increased. Extreme precipitation indices (RX1day, CDD, and SDII) also significantly increased, with most abrupt changes in 1980–1999 in the NNRHDM, NNRSCB and NNRYGP.
(3) There were stronger correlations between extreme temperature indices and NDVI than for the extreme precipitation indices in the three subregions. Additionally, the significant positive correlation for lagged 0–2 months converted to lagged 3–6 months negative correlation in different buffer areas of the three subregions. On the annual scale, extreme climate indices (FD0, ID0, CSDI, TMINmean, TR20, and WSDI) explained 92 % of NDVI change in the 5 km buffer area in the NNRYGP. On the monthly scale, DTR, TMINmean, TN10P, TN90P, TNn, TX90P, TXn, and TXx together explained 83 % of NDVI change in the NNRYGP for a 2 km buffer area, more than that explained in the NNRHDM and NNRSCB. The extraction of NDVI in different buffer zones around the stations may affect correlations between vegetation and extreme climate indices, and may lead to differences in extreme climate indices combinations that explain NDVI changes. This limitation of analysis must be considered in future research.

CRediT authorship contribution statement

Ping Wang: Conceptualization, Writing – original draft, Writing – review & editing. **Qingping Cheng:** Conceptualization, Writing – original draft, Methodology, Validation, Writing – review & editing. **Hanyu Jin:** Methodology, Validation, Data curation, Formal analysis.

Declaration of Competing Interest

The authors declare that they have no known competing financial interests or personal relationships that could have appeared to influence the work reported in this paper.

Data availability

The data that has been used is confidential.

Acknowledgements

This study was supported by the supported by Yunnan Fundamental Research Projects (Grant No. 202301BD070001-093, 202301AT070227, 202201AU70064), Southwest Forestry University Campus level Launch Fund(01102/112105).

Appendix A. Supplementary data

Supplementary data to this article can be found online at https://doi.org/10.1016/j.ecolind.2023.110247.

References

Alexander, L.V., Zhang, X., Peterson, T.C., Caesar, J., Gleason, B., Klein Tank, A.M.G., Haylock, M., Collins, D., Trewin, B., Rahimzadeh, F., 2006. Global observed changes in daily climate extremes of temperature and precipitation. J. Geophys. Res. Atmos. 111 https://doi.org/10.1029/2005JD006290.

Asamoah, E.F., Beaumont, L.J., Maina, J.M., 2021. Climate and land-use changes reduce the benefits of terrestrial protected areas. Nat. Clim. Chang 11 (12), 1105–1110. https://doi.org/10.1038/s41558-021-01223-2.

Ɓegúe, A., Vintrou, E., Ruelland, D., Claden, M., Dessay, N., 2011. Can a 25-year trend in Soudano-Sahelian vegetation dynamics be interpreted in terms of land use change? A remote sensing approach. Glob. Environ. Change 21, 413–420. https://doi.org/10.1016/j.gloenvcha.2011.02.002.

Brandt, J.S., Butsic, V., Schwab, B., Kuemmerle, T., Radeloff, V.C., 2015. The relative effectiveness of protected areas, a logging ban, and sacred areas for old-growth forest protection in southwest China. Biol. Conserv 181, 1–8. https://doi.org/10.1016/j.biocon.2014.09.043.

Caesar, J., Alexander, L.V., Trewin, B., Tse-ring, K., Sorany, L., Vuniyayawa, V., et al., 2011. Changes in temperature and precipitation extremes over the Indo-Pacific region from 1971 to 2005. Int. J. Climatol. 31 (6), 791–801. https://doi.org/10.1002/joc.2118.

Chen, I.C., Hill, J.K., Ohlemüller, R., Roy, D.B., Thomas, C.D., 2011. Rapid range shifts of species associated with high levels of climate warming. Science 333 (6045), 1024–1026. https://doi.org/10.1126/science.1206432.

Chen, H.P., Sun, J.Q., 2017. Contribution of human influence to increased daily precipitation extremes over China. Geophys. Res. Lett. 44 (5), 2436–2444. https://doi.org/10.1002/2016GL072439.

Chen, X., Wang, S.S., Hu, Z.Y., Zhou, Q.M., Hu, Q., 2018. Spatiotemporal characteristics of seasonal precipitation and their relationships with ENSO in Central Asia during 1901–2013. J. Geogr. Sci. 28 (9), 1341–1368. https://doi.org/10.1007/s11442-018-1529-2.

Cheng, Q., Gao, L., Zuo, X., Zhong, F., 2019. Statistical analyses of spatial and temporal variabilities in total, daytime, and nighttime precipitation indices and of extreme dry/wet association with large-scale circulations of Southwest China, 1961–2016. Atmos. Res. 219, 166–182. https://doi.org/10.1016/j.atmosres.2018.12.033.

Cheng, Q., Zhong, F., Wang, P., 2021. Potential linkages of extreme climate events with vegetation and large-scale circulation indices in an endorheic river basin in northwest China. Atmos. Res. 247, 105256 https://doi.org/10.1016/j.atmosres.2020.105256.

Cheng, Q., Jin, H., Ren, Y., 2023. Persistent and non-persistent regional extreme total, daytime, and nighttime precipitation events over Southwest China (1961–2019). Int. J. Climatol 1–25. https://doi.org/10.1002/joc.7968.

Ding, Y., Xu, J., Wang, X., Peng, X., Cai, H., 2020. Spatial and temporal effects of drought on Chinese vegetation under different coverage levels. Sci. Total Environ. 716 https://doi.org/10.1016/j.scitotenv.2020.137166.

Donat, M.G., Lowry, A.L., Alexander, L.V., O'Gorman, P.A., Maher, N., 2016. More extreme precipitation in the world's dry and wet regions. Nat. Clim. Chang. 6, 508–513. https://doi.org/10.1038/nclimate2941.

Elsen, P.R., Monahan, W.B., Dougherty, E.R., Merenlender, A.M., 2020. Keeping pace with climate change in global terrestrial protected areas. Sci. adv. 6 (25), eaay0814. https://doi.org/10.1126/sciadv.aay0814.

Fioravanti, G., Piervitali, E., Desiato, F., 2016. Recent changes of temperature extremes over Italy: an index-based analysis. Theor. Appl. Climatol. 123, 473–486. https://doi.org/10.1007/s00704-014-1362-1.

Fischer, E.M., Beyerle, U., Knutti, R., 2013. Robust spatially aggregated projections of climate extremes. Nat. Clim. Chang. 3, 1033–1038. https://doi.org/10.1038/nclimate2051.

Gao, X., Huang, X., Lo, K., Dang, Q., Wen, R., 2021. Vegetation responses to climate change in the Qilian Mountain Nature Reserve, Northwest China. Glob. Ecol. Conserv. 28, e01698. https://doi.org/10.1016/j.gecco.2021.e01698.

Gao, M., Piao, S., Chen, A., Yang, H., Liu, Q., Fu, Y.H., Janssens, I.A., 2019. Divergent changes in the elevational gradient of vegetation activities over the last 30 years. Nat. commun 10 (1), 2970. https://doi.org/10.1038/s41467-019-11035-w.

Garcia, R.A., Cabeza, M., Rahbek, C., Araújo, M.B., 2014. Multiple dimensions of climate change and their implications for biodiversity. Science 344 (6183), 1247579. https://doi.org/10.1126/science.1247579.

Gu, Z., Duan, X., Shi, Y., Li, Y., Pan, X., 2018. Spatiotemporal variation in vegetation coverage and its response to climatic factors in the Red River Basin. China. Ecol. Indic. 93, 54–64. https://doi.org/10.1016/j.ecolind.2018.04.033.

Hao, J., Chen, X., Zhang, Z., Gao, Y., Li, L., Li, H., 2021. Quantifying the temporal-spatial scale dependence of the driving mechanisms underlying vegetation coverage in coastal wetlands. Catena. 204, 105435 https://doi.org/10.1016/j.catena.2021.105435.

Huo, H., Sun, C., 2021. Spatiotemporal variation and influencing factors of vegetation dynamics based on Geodetector: A case study of the northwestern Yunnan Plateau. China. Ecol. Indic. 130, 108005 https://doi.org/10.1016/j.ecolind.2021.108005.

Jiang, S., Chen, X., Smettem, K., Wang, T., 2021b. Climate and land use influences on changing spatiotemporal patterns of mountain vegetation cover in southwest China. Ecol. Indic. 121, 107193 https://doi.org/10.1016/j.ecolind.2020.107193.

Jiang, Y., Shi, B., Su, G., Lu, Y., Li, Q., Meng, J., Ding, Y., Song, S., Dai, L., 2021a. Spatiotemporal analysis of ecological vulnerability in the Tibet Autonomous Region based on a pressure-state-response-management framework. Ecol. Indic. 130, 108054 https://doi.org/10.1016/j.ecolind.2021.108054.

Jones, B., O'Neill, B.C., McDaniel, L., McGinnis, S., Mearns, L.O., Tebaldi, C., 2015. Future population exposure to US heat extremes. Nat. Clim. Chang. 5, 652–655. https://doi.org/10.1038/nclimate2631.

Kreft, H., Jetz, W., 2007. Global patterns and determinants of vascular plant diversity. Proc. Natl. Acad. Sci. U.S.A. 104 (14), 5925–5930. https://doi.org/10.1073/pnas.060836110.

Kutner, M.H., Nachtsheim, C.J., Neter, J., Wasserman, W., 2004. Applied linear regression models. McGraw-Hill/Irwin New York.

Lamchin, M., Lee, W.-K., Jeon, S.W., Wang, S.W., Lim, C.H., Song, C., Sung, M., 2018. Long-term trend and correlation between vegetation greenness and climate variables in Asia based on satellite data. Sci. Total Environ. 618, 1089–1095. https://doi.org/10.1016/j.scitotenv.2017.09.145.

Lavell, A., Oppenheimer, M., Diop, C., Hess, J., Lempert, R., Li, J., Myeong, S., 2012. Managing the risks of extreme events and disasters to advance climate change adaptation. A Spec. Rep. Work. Groups I II Intergov. Panel Clim. Chang. 25–64.

Li, H., Jiang, J., Chen, B., Li, Y., Xu, Y., Shen, W., 2016. Pattern of NDVI-based vegetation greening along an altitudinal gradient in the eastern Himalayas and its response to global warming. Environ. Monit. Assess. 188, 1–10. https://doi.org/10.1007/s10661-016-5196-4.

Li, X., Li, Y., Chen, A., Gao, M., Slette, I.J., Piao, S., 2019. The impact of the 2009/2010 drought on vegetation growth and terrestrial carbon balance in Southwest China. Agric. For. Meteorol. 269, 239–248. https://doi.org/10.1016/j.agrformet.2019.01.036.

Li, Y., Piao, S., Li, L.Z.X., Chen, A., Wang, X., Ciais, P., Huang, L., Lian, X., Peng, S., Zeng, Z., Wang, K., Zhou, L., 2018b. Divergent hydrological response to large-scale afforestation and vegetation greening in China. Sci. Adv. 4, 1–10. https://doi.org/10.1126/sciadv.aar4182.

Li, Y., Song, Z., 2022. Have protected areas in China achieved the ecological and economic "win-win" goals? Evidence from the Giant Panda Reserves of the Min Mont Range. For. Policy. Econ 144, 102845. https://doi.org/10.1016/j.forpol.2022.102845.

Li, X., Wu, P., Guo, F., Hu, X., 2021. A geographically weighted regression approach to detect divergent changes in the vegetation activity along the elevation gradients over the last 20 years. For. Ecol. Manage. 490, 119089 https://doi.org/10.1016/j.foreco.2021.119089.

Li, L., Zhang, Y., Liu, L., Wu, J., Wang, Z., Li, S., Zhang, H., Zu, J., Ding, M., Paudel, B., 2018a. Spatiotemporal patterns of vegetation greenness change and associated climatic and anthropogenic drivers on the Tibetan Plateau during 2000–2015. Remote Sens. 10, 1–16. https://doi.org/10.3390/rs10101525.

Liu, H., Jiao, F., Yin, J., Li, T., Gong, H., Wang, Z., Lin, Z., 2020. Nonlinear relationship of vegetation greening with nature and human factors and its forecast–a case study of Southwest China. Ecol. Indic. 111, 106009 https://doi.org/10.1016/j.ecolind.2019.106009.

Liu, M., Xu, X., Sun, A.Y., Wang, K., Liu, W., Zhang, X., 2014. Is southwestern China experiencing more frequent precipitation extremes? Environ. Res. Lett. 9, 64002. https://doi.org/10.1088/1748-9326/9/6/064002.

Liu, Y., You, C., Zhang, Y., Chen, S., Zhang, Z., Li, J., Wu, Y., 2021. Resistance and resilience of grasslands to drought detected by SIF in inner Mongolia. China. Agric. For. Meteorol. 308–309 https://doi.org/10.1016/j.agrformet.2021.108567.

Liu, H., Zhang, M., Lin, Z., Xu, X., 2018. Spatial heterogeneity of the relationship between vegetation dynamics and climate change and their driving forces at multiple time scales in Southwest China. Agric. For. Meteorol. 256, 10–21. https://doi.org/10.1016/j.agrformet.2018.02.015.

Loarie, S.R., Duffy, P.B., Hamilton, H., Asner, G.P., Field, C.B., Ackerly, D.D., 2009. The velocity of climate change. Nature 462 (7276), 1052–1055. https://doi.org/10.1038/nature08649.

Ma, Y., Zuo, L., Gao, J., Liu, Q., Liu, L., 2021. The karst NDVI correlation with climate and its BAS-BP prediction based on multiple factors. Ecol. Indic. 132, 108254 https://doi.org/10.1016/j.ecolind.2021.108254.

Ma, Y., Guan, Q., Sun, Y., Zhang, J., Yang, L., Yang, E., Li, H., Du, Q., 2022. Three-dimensional dynamic characteristics of vegetation and its response to climatic factors in the Qilian Mountains. Catena 208, 105694. https://doi.org/10.1016/j.catena.2021.105694.

Mann, H.B., 1945. Nonparametric tests against trend. Econometrica 133, 245–259.

Meehl, G.A., Tebaldi, C., Walton, G., Easterling, D., McDaniel, L., 2009. Relative increase of record high maximum temperatures compared to record low minimum temperatures in the US. Geophys. Res. Lett. 36 https://doi.org/10.1029/2009GL040736.

Naidoo, R., Gerkey, D., Hole, D., Pfaff, A., Ellis, A.M., Golden, C.D., Herrera, D., Johnson, K., Mulligan, M., T. Ricketts, H., Fisher, B., 2019. Evaluating the impacts of protected areas on human well-being across the developing world. Sci. Adv. 5 (4), eaav3006. https://doi.org/10.1126/sciadv.aav3006.

Ohlemüller, R., 2011. Running out of climate space. Science 334 (6056), 613–614. https://doi.org/10.1126/science.1214215.

Ouyang, W., Wu, Y., Hao, Z., Zhang, Q., Bu, Q., Gao, X., 2018. Combined impacts of land use and soil property changes on soil erosion in a mollisol area under longterm agricultural development. Sci. Total Environ. 613, 798–809. https://doi.org/10.1016/j.scitotenv.2017.09.173.

Ouyang, W., Wan, X., Xu, Y., Wang, X., Lin, C., 2020. Vertical difference of climate change impacts on vegetation at temporal-spatial scales in the upper stream of the Mekong River Basin. Sci. Total Environ. 701, 134782 https://doi.org/10.1016/j.scitotenv.2019.134782.

Panthou, G., Vischel, T., Lebel, T., Blanchet, J., Quantin, G., Ali, A., 2012. Extreme rainfall in West Africa: A regional modeling. Water Resour. Res. 48, 682–688. https://doi.org/10.1029/2012WR012052.

Papalexiou, S.M., Montanari, A., 2019. Global and regional increase of precipitation extremes under global warming. Water Resour. Res. 55, 4901–4914. https://doi.org/10.1029/2018WR024067.

Papalexiou, S.M., AghaKouchak, A., Trenberth, K.E., Foufoula-Georgiou, E., 2018. Global, regional, and megacity trends in the highest temperature of the year: Diagnostics and evidence for accelerating trends. Earth's Futur. 6, 71–79. https://doi.org/10.1002/2017EF000709.

Peng, W., Kuang, T., Tao, S., 2019. Quantifying influences of natural factors on vegetation NDVI changes based on geographical detector in Sichuan, western China. J. Clean. Prod. 233, 353–367. https://doi.org/10.1038/nature12434.

Peng, S., Piao, S., Ciais, P., Myneni, R.B., Chen, A., Chevallier, F., Dolman, A.J., Janssens, I.A., Penuelas, J., Zhang, G., 2013. Asymmetric effects of daytime and night-time warming on Northern Hemisphere vegetation. Nature. 501, 88–92. https://doi.org/10.1038/nature12434.

Perkins, S.E., Alexander, L. V, Nairn, J.R., 2012. Increasing frequency, intensity and duration of observed global heatwaves and warm spells. Geophys. Res. Lett. 39 ((20)), l20714-1-l20714-5. http://doi.org/10.1029/2012GL053361.

Pettitt, A.N., 1979. A non-parametric approach to the change-point problem. App. Statis. 28 (2), 126–135.

Pfahl, S., O'Gorman, P.A., Fischer, E.M., 2017. Understanding the regional pattern of projected future changes in extreme precipitation. Nat. Clim. Chang. 7, 423–427. https://doi.org/10.1038/nclimate3287.

Piao, S., Mohammat, A., Fang, J., Cai, Q., Feng, J., 2006. NDVI-based increase in growth of temperate grasslands and its responses to climate changes in China. Global. Environ. Chang 16 (4), 340–348. https://doi.org/10.1016/j.gloenvcha.2006.02.002.

Qin, N., Wang, J., Yang, G., Chen, X., Liang, H., Zhang, J., 2015. Spatial and temporal variations of extreme precipitation and temperature events for the Southwest China in 1960–2009. Geoenviron. Disat. 2, 1–14. https://doi.org/10.1186/s40677-015-0014-9.

Rahmstorf, S., Coumou, D., 2011. Increase of extreme events in a warming world. Proc. Natl. Acad. Sci. 108, 17905–17909. https://doi.org/10.2307/41352625.

Scheffers, B.R., De Meester, L., Bridge, T.C., Hoffmann, A.A., Pandolfi, J.M., Corlett, R.T., Butchart, S.H.M., Pearce-Kelly, P., Kovacs, K.M., Dudgeon, D., Pacifici, M., Rondinini, C., Foden, W.B., Martin, T.G., Mora, C., Bickford, D., Watson, J.E., 2016. The broad footprint of climate change from genes to biomes to people. Science 354 (6313), aaf7671. https://doi.org/10.1126/science.aaf7671.

Schoof, J.T., Robeson, S.M., 2016. Projecting changes in regional temperature and precipitation extremes in the United States. Weather Clim. Extremes 11, 28–40. https://doi.org/10.1016/j.wace.2015.09.004.

Sen, P.K., 1968. Estimates of the regression coefficient based on Kendall's tau. J. Am. Stat. Assoc. 39, 1379–1389.

Shao, H., Zhang, Y., Gu, F., Shi, C., Miao, N., Liu, S., 2021. Impacts of climate extremes on ecosystem metrics in southwest China. Sci. Total Environ. 776, 145979 https://doi.org/10.1016/j.scitotenv.2021.145979.

Shen, X., Liu, B., Jiang, M., Wang, Y., Wang, L., Zhang, J., Lu, X., 2021. Spatiotemporal change of marsh vegetation and its response to climate change in China from 2000 to 2019. J. Geophys. Res-Biogeo, 126, e2020JG006154. 10.1029/2020JG006154.

Shrestha, N., Xu, X., Meng, J., Wang, Z., 2021. Vulnerabilities of protected lands in the face of climate and human footprint changes. Nat. Commun. 12, 1–9. https://doi.org/10.1038/s41467-021-21914-w.

Siepielski, A.M., Morrissey, M.B., Buoro, M., Carlson, S.M., Caruso, C.M., Clegg, S.M., Coulson, T., DiBattista, J., Gotanda, K.M., Francis, C.D., 2017. Precipitation drives global variation in natural selection. Science. 355 (6328), 959–962. https://doi.org/10.1126/science.aag2773.

Smith, A.M.S., Kolden, C.A., Tinkham, W.T., Talhelm, A.F., Marshall, J.D., Hudak, A.T., Boschetti, L., Falkowski, M.J., Greenberg, J.A., Anderson, J.W., Kliskey, A., Alessa, L., Keefe, R.F., Gosz, J.R., 2014. Remote sensing the vulnerability of vegetation in natural terrestrial ecosystems. Remote Sens. Environ. 154, 322–337. https://doi.org/10.1016/j.rse.2014.03.038.

Song, L., Li, Y., Ren, Y., Wu, X., Guo, B., Tang, X., Shi, W., Ma, M., Han, X., Zhao, L., 2019. Divergent vegetation responses to extreme spring and summer droughts in Southwestern China. Agric. For. Meteorol. 279, 107703 https://doi.org/10.1016/j.agrformet.2019.107703.

Sun, H., Wang, X., Fan, D., Sun, O.J., 2022. Contrasting vegetation response to climate change between two monsoon regions in Southwest China: The roles of climate condition and vegetation height. Sci. Total Environ. 802, 149643 https://doi.org/10.1016/j.scitotenv.2021.149643.

Sun, Y., Zhang, X.B., Zwiers, F.W., Song, L.C., Wan, H., Hu, T., et al., 2014. Rapid increase in the risk of extreme summer heat in eastern China. Nat. Clim. Change. 4 (12), 1082–1085. https://doi.org/10.1038/nclimate2410.

Sun, Y., Zhang, X., Ren, G., Zwiers, F.W., Hu, T., 2016. Contribution of urbanization to warming in China. Nat. Clim. Chang. 6, 706–709. https://doi.org/10.1038/nclimate2956.

Sun, Y., Guan, Q., Wang, Q., Yang, L., Pan, N., Ma, Y., Luo, H., 2021. Quantitative assessment of the impact of climatic factors on phenological changes in the Qilian Mountains. China. For. Eco. Manage 499, 119594. https://doi.org/10.1016/j.foreco.2021.119594.

Tan, Z., Tao, H., Jiang, J., Zhang, Q., 2015. Influences of climate extremes on NDVI (normalized difference vegetation index) in the Poyang Lake Basin, China. Wetlands 35, 1033–1042. https://doi.org/10.1007/s13157-015-0692-9.

Tao, J., Xu, T., Dong, J., Yu, X., Jiang, Y., Zhang, Y., Huang, K., Zhu, J., Dong, J., Xu, Y., 2018. Elevation-dependent effects of climate change on vegetation greenness in the high mountains of southwest China during 1982–2013. Int. J. Climatol. 38, 2029–2038. https://doi.org/10.1007/s13157-015-0692-9.

Theil, H., 1950. A rank-invariant method of linear and polynomial regression analysis. Indag. Math. 12, 173.

Watson, J.E., Iwamura, T., Butt, N., 2013. Mapping vulnerability and conservation adaptation strategies under climate change. Nat. Clim. Change 3 (11), 989–994. https://doi.org/10.1038/nclimate2007.

Wei, S.K., Fan, S.X., Zhang, Y.Z., Huang, X.R., Zhang, Z.D., 2018. Vegetation dynamic trends and the main drivers detected using the ensemble empirical mode decomposition method in East Africa. Land Degrad. Dev. 29, 2542–2553. https://doi.org/10.1002/ldr.3017.

Wen, Z., Wu, S., Chen, J., Lü, M., 2017. NDVI indicated long-term interannual changes in vegetation activities and their responses to climatic and anthropogenic factors in the Three Gorges Reservoir Region. China. Sci. Total Environ. 574, 947–959. https://doi.org/10.1016/j.scitotenv.2016.09.049.

Westra, S., Alexander, L.V., Zwiers, F.W., 2013. Global increasing trends in annual maximum daily precipitation. J. Clim. 26, 3904–3918. https://doi.org/10.1175/jcli-d-12-00502.1.

Williams, J.W., Jackson, S.T., 2007. Novel climates, no-analog communities, and ecological surprises. Front. Ecol. Environ. 5 (9), 475–482. https://doi.org/10.1890/070037.

Woodward, F.I., Lomas, M.R., Kelly, C.K., 2004. Global climate and the distribution of plant biomes. Philos. Trans. R. Soc. Lond. B Biol 359 (1450), 1465–1476. https://doi.org/10.1098/rstb.2004.1525.

Wu, H., Fang, S., Yu, L., Hu, S., Chen, X., Cao, Y., Ma, K., 2023. Limited co-benefits of protected areas in southwest China under current climate change and human modification. J. Environ. Manage 330, 117190. https://doi.org/10.1016/j.jenvman.2022.117190.

Wu, D., Zhao, X., Liang, S., Zhou, T., Huang, K., Tang, B., Zhao, W., 2015. Time-lag effects of global vegetation responses to climate change. Glob. Chang. Biol. 21, 3520–3531. https://doi.org/10.1111/gcb.12945.

Xu, X., Huang, A., Belle, E., De Frenne, P., Jia, G., 2022. Protected areas provide thermal buffer against climate change. Sci. Adv. 8 (44), eabo0119. https://doi.org/10.1126/sciadv.abo0119.

Xu, B., Gong, P., Pu, R., 2003. Crown closure estimation of oak savannah in a dry season with Landsat TM imagery: comparison of various indices through correlation analysis. Int. J. Remote Sens. 24, 1811–1822. https://doi.org/10.1080/01431160210144598.

Xu, S., Yu, Z., Lettenmaier, D.P., McVicar, T.R., Ji, X., 2020. Elevation-dependent response of vegetation dynamics to climate change in a cold mountainous region. Environ. Res. Lett. 15, 094005 https://doi.org/10.1088/1748-9326/ab9466.

Xue, T.T., Tang, G.P., Sun, L., Wu, Y.Z., Liu, Y.L., Dou, Y.F., 2017. Long-term trends in precipitation and precipitation extremes and underlying mechanisms in the U.S. Great Basin during 1951–2013. J. Geophys. Res-Atmosp. 122 (12), 6152–6169. https://doi.org/10.1002/2017JD026682.

Yan, W., Wang, H., Jiang, C., Jin, S., Ai, J., Sun, O.J., 2021. Satellite view of vegetation dynamics and drivers over southwestern China. Ecol. Indic. 130, 108074 https://doi.org/10.1016/j.ecolind.2021.108074.

Yin, L., Dai, E., Zheng, D., Wang, Y., Ma, L., Tong, M., 2020. What drives the vegetation dynamics in the Hengduan Mountain region, southwest China: Climate change or human activity? Ecol. Indic. 112, 106013 https://doi.org/10.1016/j.ecolind.2019.106013.

Ying, H., Zhang, H., Zhao, J., Shan, Y., Zhang, Z., Guo, X., Deng, G., 2020. Effects of spring and summer extreme climate events on the autumn phenology of different vegetation types of Inner Mongolia, China, from 1982 to 2015. Ecol. Indic. 111, 105974 https://doi.org/10.1016/j.ecolind.2019.105974.

Yue, S., Wang, C.Y., 2002. Applicability of prewhitening to eliminate the influence of serial correlation on the Mann-Kendall test. Water Resour. Res. 38, 1–4. https://doi.org/10.1029/2001wr000861.

Zhang, W., Liu, L., Song, K., Li, X., Wang, Y., Tang, Y., Jiang, H., 2019. Remote sensing the orographic effects of dry-hot valley on vegetation distribution in the southeast Tibetan Plateau. Int. J. Remote Sens. 40, 8589–8607. https://doi.org/10.1080/01431161.2019.1620370.

Zhang, C., Wu, S.H., 2021. An analysis on moisture source of extreme precipitation in Southwest China in summer. J Nat. Resour 36, 1186–1194. https://doi.org/10.31497/zrzyxb.20210508.

Zhou, P., Liu, Z.Y., 2018. Likelihood of concurrent climate extremes and variations over China. Environ. Res. Lett. 13 (9), 094023 https://doi.org/10.1088/1748-9326/aade9e.094023.